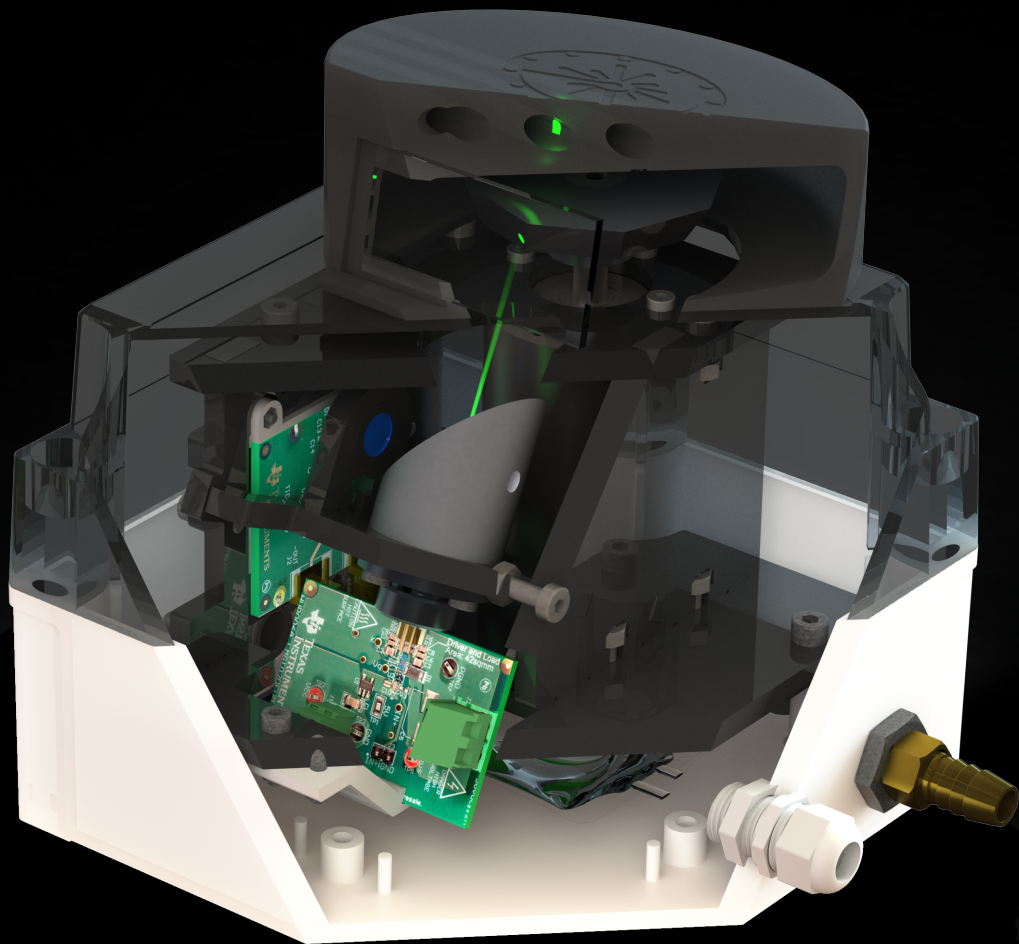


# Design of a Deep Sea LiDAR system

Laser Pulse Transmission





# Design of a Deep Sea LiDAR system

## Laser Pulse Transmission BSc Thesis

Authors:	L.R Wix	4534654
	E.P.M Zwetsloot	4583817
Project duration:	February 11 - July 5, 2019	
Supervisor:	Prof. Dr. Ir. G.J.T. Leus	
Thesis committee:	Prof. Dr. Ir. G.J.T. Leus	
	Prof. Dr. Ir. K.L.M. Bertels	
	Dr. F. Uysal	
	Ing. F. van der Zwan	
	Dr. D. Elkouss Coronas	

With contributions from the entire electrical engineering work group of the SLiDAR team in chapter 2.  
*Bsc. Electrical Engineering 2019 BAP group A :*

A.E. Admiraal	4545532
J. Jonk	4577221
B. Minderman	4577868
B.M. Verdoes	4563263
L.R. Wix	4534654
E.P.M. Zwetsloot	4583817

This work builds on ideas from the mechanical engineering work group of the SLiDAR team.  
*Bsc. Mechanical Engineering 2019 BEP group A2 :*

D. Looman  
S.H.R. Rutten  
B.R. van Vliet  
D.O. Wijnberg

In partial fulfilment of the requirements for the degree of

**Bachelor of Science**  
in Electrical Engineering

at the Delft University of Technology.

An electronic copy of this thesis is available at <https://repository.tudelft.nl/>.





# Abstract

Current subsea LiDAR implementations are inherently depth limited, and make LiDAR applications in the deep-sea costly. To this end, the SLiDAR project aims to develop a pressure tolerant LiDAR system for use at any ocean depth. This thesis elaborates the design and implementation of the laser pulse transmission of the LiDAR and the circuit which will supply the bias voltage for the Avalanche photodiode (APD) from the receiving stage. Although testing of the transmission stage showed the laser can be pulsed, there can be more optimizations done in the future as better laser system can be designed to achieve higher optical output power and an even smaller pulse width. Furthermore, future optimizations should be considered for the APD bias circuit as there were some minor problems in the PCB. Unfortunately, the LiDAR system as a whole was not tested in practise, due to time limitations. Hence, this thesis aims to provide a basis for future development, testing and verification of both the LiDAR system and its laser pulse transmission stage.



# Preface

The Subsea LiDAR (SLiDAR) is a multidisciplinary Bachelor Graduation Project. The project team consists of 6 Bachelor of Electrical Engineering students and 4 Bachelor of Mechanical Engineering students. The idea for the project stems from the need of a ranging sensor on the Life OBserving Sea Traversing Explorer Robot (LOBSTER). The initial goal was to design a 3D laser scanning device based on the LiDAR principle that could work in the deep sea environment. As of writing this thesis, the design is left partially unfinished due to the large work load.

This thesis is one of a series of three theses on the electrical system design of the SLiDAR project. Each thesis is written by a subgroup of two project members, who implemented a specific subsystem of the LiDAR. Every thesis starts of with an almost identical chapter on the system design of the LiDAR. After that follows a chapter on the design of the subgroup specific subsystem.

We would like to thank Prof. Dr. Ir. G.J.T. Leus for supervising the project, and our sponsor. Furthermore we would like to thank the MacArtney Group for letting us use their facilities for a reduced price. Finally, we would like to thank all members of the SLiDAR team for their efforts and enjoyable collaboration.

*Lynrick Wix & Eva Zwetsloot*

*Delft, June 2019*



# Contents

<b>1</b>	<b>Introduction</b>	<b>1</b>
<b>2</b>	<b>SLiDAR System Design</b>	<b>3</b>
2.1	Current underwater ranging methods . . . . .	3
2.2	A simple LiDAR system . . . . .	5
2.3	Functions of LiDAR systems . . . . .	5
2.3.1	Channel estimation and target detection . . . . .	5
2.3.2	The abstract channel & sample distribution . . . . .	6
2.3.3	Towards a Functional Breakdown Structure (FBS) . . . . .	6
2.4	Requirements. . . . .	6
2.4.1	Towards a Requirement Discovery Tree (RDT) . . . . .	6
2.4.2	Programme of Requirements . . . . .	7
2.5	Design options . . . . .	9
2.5.1	Distribution . . . . .	9
2.5.2	Channel estimation . . . . .	10
2.5.3	Target detection. . . . .	11
2.5.4	Digitisation . . . . .	12
2.5.5	Design Option Tree (DOT) . . . . .	12
2.6	Concept selection . . . . .	12
2.6.1	Distribution . . . . .	12
2.6.2	Channel estimation . . . . .	13
2.6.3	Digitisation method . . . . .	13
2.6.4	Target detection. . . . .	14
2.7	Subsystem selection . . . . .	14
2.8	System modelling. . . . .	14
2.8.1	Towards a simple model . . . . .	15
2.8.2	Channel impulse response. . . . .	15
2.8.3	Towards wavelength requirements . . . . .	16
2.8.4	Towards power & input sensitivity requirements . . . . .	16
2.8.5	Towards bandwidth requirements . . . . .	16
2.9	Functional Overview . . . . .	17
2.9.1	Functional flow . . . . .	17
2.9.2	Interface specification . . . . .	18
<b>3</b>	<b>Program of requirements</b>	<b>21</b>
<b>4</b>	<b>Design of TX stage</b>	<b>23</b>
4.1	Light element . . . . .	23
4.1.1	Laser vs LED . . . . .	23
4.1.2	Laser types . . . . .	23
4.1.3	Semiconductor laser . . . . .	24
4.1.4	Frequency doubling crystal . . . . .	24
4.2	Optical Amplifier . . . . .	24
4.3	Laser driver . . . . .	25
4.3.1	Schematic. . . . .	25
4.4	Pulse generator. . . . .	26
4.4.1	Option A: Transmission line . . . . .	26
4.4.2	Option B: XOR and RC configuration . . . . .	27
4.4.3	Option C: Double XOR configuration . . . . .	27
4.4.4	Option D: IC Delay line. . . . .	27
4.4.5	Option E: Comparator configuration . . . . .	28
4.5	Power converters . . . . .	28
4.5.1	Bus voltage . . . . .	29
4.5.2	Bias voltage. . . . .	29
4.5.3	APD bias voltage . . . . .	29

<b>5</b>	<b>Implementation</b>	<b>31</b>
5.1	Laser Diode . . . . .	31
5.1.1	Pressure tolerance . . . . .	31
5.1.2	Focusing lens and heatsink . . . . .	31
5.2	Laser driver . . . . .	32
5.2.1	Micro vias . . . . .	32
5.2.2	Pulse generator. . . . .	32
5.3	Bus voltage . . . . .	32
5.4	Bias voltage. . . . .	33
5.5	APD bias voltage . . . . .	34
5.5.1	Schematic. . . . .	34
<b>6</b>	<b>Testing and Validation</b>	<b>37</b>
6.1	Laser diode . . . . .	37
6.1.1	Pressure tolerance integration . . . . .	37
6.1.2	Pressure test of the laser diode . . . . .	37
6.2	Pulse generator. . . . .	38
6.3	Bus and bias voltage . . . . .	38
6.4	Laser driver . . . . .	39
6.4.1	Inductive overshoot. . . . .	39
6.4.2	Optical output power . . . . .	39
6.5	APD bias voltage . . . . .	40
<b>7</b>	<b>Conclusion</b>	<b>41</b>
7.1	Future work . . . . .	41
7.1.1	Transmit stage . . . . .	41
7.1.2	LiDAR. . . . .	42
<b>A</b>	<b>Appendix</b>	<b>47</b>
A.1	Matlab script for range estimation . . . . .	47
A.2	Transmission field integral . . . . .	48
A.3	The polygon. . . . .	48
A.4	Beam divergence. . . . .	50
A.5	Laser . . . . .	50
A.6	Optical Amplifiers. . . . .	51
A.7	Laser driver of TI test results. . . . .	52
A.8	Diodes. . . . .	52
A.9	Power converters . . . . .	53
A.9.1	Linear mode . . . . .	53
A.9.2	Switching mode. . . . .	54
A.9.3	Resonant mode. . . . .	55
A.10	APD boost converter . . . . .	55
A.11	Pulse generator simulation. . . . .	55
A.12	Explanation of the frequency doubling [10] . . . . .	55
A.13	Derivation for the component values for the buck converter, Bias voltage. . . . .	56
A.13.1	VIN and EN pin . . . . .	57
A.13.2	PGOOD pin. . . . .	57
A.13.3	SS pin. . . . .	57
A.13.4	RT pin. . . . .	58
A.13.5	HYS pin . . . . .	58
A.13.6	SW pin . . . . .	58
A.13.7	ILIM pin . . . . .	58
A.13.8	VOUT pin . . . . .	58
A.14	Derivation of the component values for the linear regulator, Bus voltage . . . . .	58
A.14.1	Requirements. . . . .	59
A.14.2	Resistor network . . . . .	59
A.14.3	Input and output capacitor . . . . .	60
A.15	PCB implementation of the deliverables. . . . .	60
A.15.1	PCB for the laser driver and bias voltage . . . . .	60
A.15.2	PCB for the bus voltage . . . . .	60
A.15.3	PCB for the APD bias . . . . .	60

A.16 Test plan for the altered laser driver . . . . .	61
A.16.1 Goal of the test . . . . .	61
A.16.2 List of essentials . . . . .	61
A.16.3 Testplan steps . . . . .	61

## List of Abbreviations

- ADC** Analog to Digital Converter
- APD** Avalanche photodiode
- CFAR** Constant False Alarm Rate
- COTS** Commercial Off-The-Shelf
- DOT** Design Option Tree
- EDFA** Erbium Doped Fiber Amplifier
- FBS** Functional Breakdown Structure
- FOV** Field Of View
- GaN FET** Gallium Nitride MOSFET
- LLS** Laser Line Scanning
- LOBSTER** Life OBserving Sea Traversing Explorer Robot
- MEMS** MicroElectroMechanical Systems
- MOPA** Master Oscillator Power Amplifier
- MOSFET** metal-oxide-semiconductor field-effect transistor
- nMOSFET** n-channel metal-oxide-semiconductor field-effect transistor
- OPA** Optical Phased Array
- PCB** Printed Circuit Board
- RADAR** Radio Distance And Ranging
- RDT** Requirements Discovery Tree
- SfM** Structure from Motion
- SLAM** Simultaneous Localisation And Mapping
- SLiDAR** Subsea LiDAR
- SNR** Signal to Noise Ratio
- SONAR** Sound Navigation And Ranging
- SPI** Serial Peripheral Interface
- TDC** Time to Digital Converter
- TI** Texas Instruments
- ToF** Time of Flight
- VCSEL** Vertical Cavity Surface Emitting Laser



# Introduction

Although deep water ecosystems are crucially important for human interests, they remain far from being fully understood [87]. It is simply very hard to get there. One of the challenges of subsea exploration is navigation. Satellite navigation signals are quickly attenuated in seawater and acoustic beacons are costly to set up. Conventional robotic systems employ Simultaneous Localisation And Mapping (SLAM) techniques to find their position from ranging information in this absence of positional references [66]. Limitations of subsea perception sensors make this difficult in the subsea environment [28].

LiDAR systems are often used in ranging applications above sea, but are not traditionally considered for use in subsea SLAM implementations [28]. Although subsea LiDAR systems exist, it is only marketed at asset inspection and metrology. Although it has high resolution and accuracy, the maximum scan speed of  $2 \text{ min}^{-1}$  [20] and high price of €500k probably contribute to its lack of application in subsea SLAM.

The goal of the Subsea LiDAR (SLiDAR) project is to explore the feasibility of an inexpensive subsea LiDAR system optimised for SLAM. This challenge is jointly tackled by a team of four mechanical engineering students investigating mechanical problems in their bachelor thesis and a team of six electrical engineering investigating electrical aspects in their thesis.

This thesis focuses on the electrical design, which is divided over:

- the transmission stage, generating high power laser pulses;
- the receiver stage, converting the Time of Flight (ToF) of the laser pulse to a digital reading;
- a scanning stage, distributing the distance measurements in space;
- a digital system, to time the measurements and communicate them to the outside world.

The present work motivates this division in part 2.6 and then details the design of the transmit stage here after, the design in chapter 4, implementation in chapter 5 and validation of the transmit stage in chapter 6. Figure 1.1 gives an overview of the system and illustrates the scope of these parts.

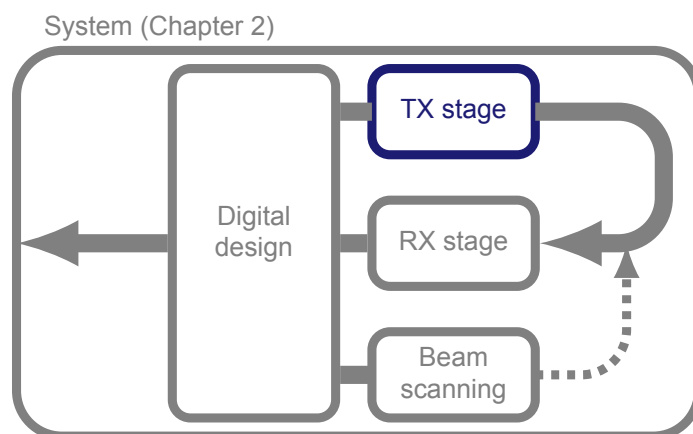


Figure 1.1: System overview.



# 2

## SLiDAR System Design

In this chapter, we explore system architectures suitable for SLAM capable deep sea LiDAR and establish a subsystem division for our implementation along with requirements on each subsystem. To this end, section 2.1 first motivates the choice to investigate deep sea LiDAR as a solution to the underwater SLAM problem by exploring its relation to current underwater ranging methods in a review of current underwater ranging methods. From there, section 2.2 will examine the system architecture of a simple LiDAR system for context, before we take the discussion to a more abstract point in section 2.3, identifying the fundamental functions of LiDAR systems. Section 2.3.3 will provide a summary of them in the form of a Functional Breakdown Structure (FBS) for a more visual overview. It will also serve as the basis of a Requirements Discovery Tree (RDT) in section 2.4.1, ensuring exhaustive coverage by requirements. Section 2.4.2 will detail them in a programme of requirements. Having established the functions of and requirements on the deep sea LiDAR, we will seek design options to fulfil these by analysing the state of the art of LiDAR techniques in section 2.5. These will be summarised in a Design Option Tree (DOT) in section 2.5.5, again providing a visual overview for further reflection. This reflection comes in the form of the selection of techniques best suited to our application to form a concept design by weighing their advantages and disadvantages in section 2.6. From here, functionalities are grouped in subsystems in section 2.7. This split generates the need for more detailed requirements on system-level key parameters. To find these, some system-level modelling is performed in section 2.8. Finally, section 2.9 gives a high-level overview of the proposed LiDAR design, and specifies the data flow on the interfaces between the made subsystems.

### 2.1. Current underwater ranging methods

This section explores the ways in which an underwater SLAM capable LiDAR could contribute to underwater SLAM by evaluating the strengths and weaknesses of current underwater ranging methods and investigating the unique role a LiDAR system could play.

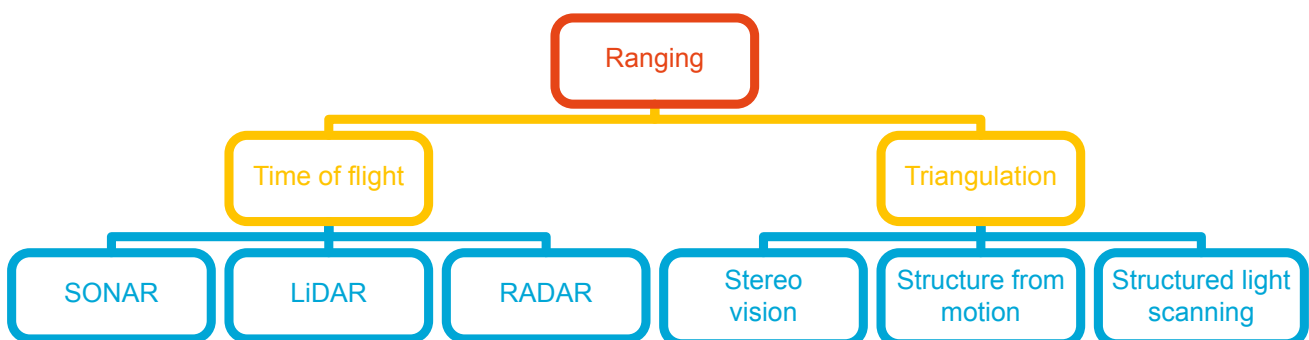


Figure 2.1: Classes of ranging methods. Adapted from [44, 34].

Current ranging methods can be classified as shown in figure 2.1. We distinguish two major classes based on the measured quantity:

- Triangulation methods estimate the distance to an object from the angles of at least two rays intersecting a certain point on an object.
- ToF methods estimate the distance to an object from the return time of an echo in a certain domain.

Triangulation methods can be further divided based on the types of angular measurements. A distinction can be made between stereo vision, structure from motion and structured light scanning. In industry, all of these systems are implemented optically. This introduces a trade-off between sensor size, sensitivity and resolution. Since sunlight does not reach the deep sea, there is also a trade-off between the sensor to illumination separation distance and interference due to volumetric backscatter.

Stereo vision uses concurrent angular measurements to a point from multiple vantage points. Any underwater can be used, from inexpensive consumer level action cameras, to machine vision cameras in \$1500 pressure housings [69] or even dedicated deepwater equipment, such as the \$60k Sulis subsea camera [80], any of the DeepSea Power & Light equipment [19] or Sidus cameras and lighting solutions [73]. Since stereo algorithms depend on detecting features of the environment, the barren seafloor can pose a challenge [52]. Nevertheless, stereo vision has been demonstrated in a natural environment at 1750 m [11]. Underwater stereo based SLAM has also been demonstrated [64], but low visibility remains an issue. Though few authors report maximum range, 10 m seems to be a good estimate based on qualitative inspection of the visual results in [64].

Structure from Motion (SfM) approaches find the 3D structure of an object through angular measurements from a great number of overlapping but unknown vantage points. They are closely related to stereo methods, also requiring significant processing. Again, any underwater camera can be used. Conventional SfM methods have been used to map coral reefs [13] and in general aquatic applications of the technology are regarded to be rapidly developing [15]. Difficulties in detecting features on the barren seafloor can again pose a challenge, but can ultimately be overcome such that underwater monocular SLAM has been demonstrated [52]. SfM approaches suffer the same limitations as stereo methods.

Structured light scanning uses a light source with a known angular distribution and measures the angles of the reflected light. Laser line scanners are common underwater structured light scanners. Examples include the Newton M310UW [53], the Kraken SeaVision [63] and the 2G Robotics ULS-500 pro [1]. Thanks to the use of laser light, excellent resolutions can be obtained down to  $0.0057^\circ$  (SeaVision). In clear water, the range is limited to 20 m (ULS-500 pro), though usually lower at 5 m (M310UW) or 8 m (SeaVision). To obtain the long range, the trade-off between low volumetric backscatter and sensor to light distance makes for a bulky 1.2 m system (ULS-500 pro). Fighting the trade-off between sensor size, sensitivity and resolution likely contribute to high system cost, \$200k for the ULS-500 pro for example. Some systems, such as the ULS-500 pro are dynamic scanners, such that they rely on the movement of the vehicle for one of their scan axes. This makes them unsuited as a sole sensor for SLAM, though still usable in the more common fusion approach.

ToF systems can be further divided based on the domain of the echo. Sound Navigation And Ranging (SONAR) systems use acoustic echos, LiDAR systems use optical echos and Radio Distance And Ranging (RADAR) systems use radio echos.

RADAR is not suited for underwater use as the signal simply attenuates too fast in water to obtain usable results. For frequencies high enough for practical antenna sizes, the attenuation of radio waves in seawater is too high to perform medium distance ranging ( $>1$  m), due to the combination of the conduction losses at low frequencies [6] and the attenuation of pure water at high frequencies [68]. This makes underwater RADAR unfeasible.

SONAR widely employed for underwater scanning, since its range is not limited by the turbidity of the water. Edgetech [23], Klein Marine [71], Coda Octopus [16], Trittech [89] and Teledyne [82] all produce a multitude of marine SONAR systems. Two SONAR techniques that are often employed are multibeam and side scan SONAR. Multibeam sonar uses phased arrays to steer the laser beam. There is also side scan SONAR. A SONAR beam orthogonal to the direction of motion of the vessel, is combined with a simple altimeter to form a map. SONAR does have its limitations. [28] points out that side scan sonar does not really provide 3D information, since the reflection intensity depends on the orientation of the surface, rather than the distance. The researcher mentions that for practical transducer sizes, the angular resolution remains limited due to the relatively large wavelength of the sound waves. For example, the \$25k Teledyne blueview has a resolution of  $1^\circ$  at a range of 10 m with up to 1 Hz update rates. The \$200k Coda Octopus Echoscope 4G boasts beam spacing down to  $0.19^\circ$  and at a range of 20 m with up to 20 Hz update rates. The Trittech Gemini 720ik has resolution of  $0.25^\circ$  at a range of 1 m and an absurd 97 Hz.

To the best of our knowledge, only one company offers underwater LiDAR. 3DAAtDepth has designed a \$500k underwater LiDAR system that has a range precision of 6 mm and an angular resolution of less than  $0.025^\circ$ . The maximum range is limited to 45 m [20]. Some authors also distinguish the INSCAN system by Teledyne CDL [24], but the 3DAAtDepth optical stage seems to have been used [40]. Thanks to the short optical wavelengths, the resolution of LiDAR is higher than SONAR. However, the scan rate is too low for SLAM applications at  $2 \text{ min}^{-1}$ . Furthermore, the range is limited by turbidity. Nevertheless, LiDAR systems can assist in increasing efficiency of bathymetry surveys, though cost remains a limiting factor [24].

Further variations are found by combining these methods. For example, Pulse Gated Laser Line Scanning (LLS) employs range gated imaging to reduce interference from backscattering in a structured light scanning method [14].

In conclusion, each underwater ranging method comes with its unique detractors. All solutions in industrial use are either expensive or very expensive. Many are inherently depth-limited because of their reliance on pressure vessels. LiDAR systems are certainly not a solution to all underwater SLAM problems, but given their prominence in regular robotics, they deserve more exploration. Low cost is an especially attractive property. A significant part of the cost of current systems can be attributed to the pressure vessel [24], which can be omitted by using pressure tolerant design techniques [54]. For these reasons, the remainder of this thesis will focus on determining the feasibility of a deep sea SLAM capable pressure tolerant LiDAR system by facing the design challenge.

## 2.2. A simple LiDAR system

Having motivated the choice to investigate deep sea capable LiDAR as a potential solution to the deep sea SLAM problem, we will now examine a simple LiDAR architecture to provide sufficient context to perform more abstract analysis in later sections.

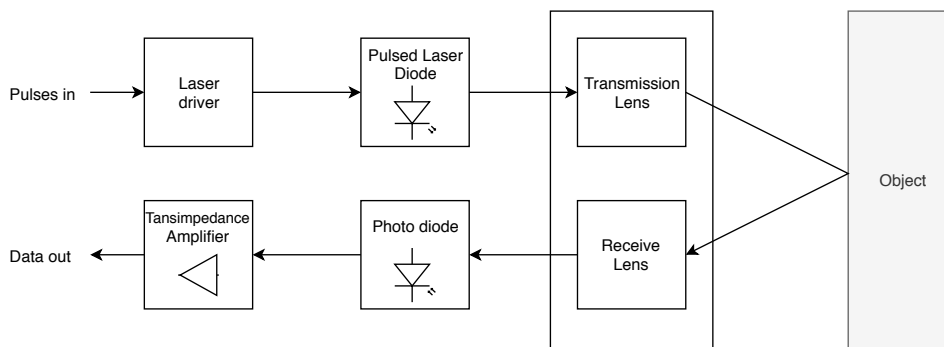


Figure 2.2: Schematic view of a simple LiDAR system, adapted from [83]

A general overview of a simplified LiDAR system can be seen in figure 2.2. The basic concept of a LiDAR system is to send out a pulse of light and measure the time it takes for the pulse to return. Assuming the propagation speed of light is known, a distance can be calculated from this time of flight. Since light spreads and attenuates over distance, the reflection is very weak. Detection is usually aided by sending out a very bright flash of light. The light is also commonly focussed to a tight, collimated beam. This ensures that all the light is reflected from a single target of interest. Laser diodes are commonly used as a means of providing fast light pulses. In most cases, a wavelength is chosen that is not dominantly present in sunlight. This minimises interference.

Generally, the creation of a light pulse is preceded by a timing system generating a pulse with the correct width and at the correct time. This signal generally does not have the signal strength to power the laser, so a laser driver is used. It amplifies the incoming pulses so that the laser diode receives sufficient power to shine brightly. When the light leaves the system, the light gets focused by a lens to obtain a collimated beam. The entire LiDAR system is usually rotated to scan the beam the environment using a gimbal. This ensures that a depth map can be built of the environment - not just a single point.

Once the laser beam hits an object, a small portion of light will reflect back towards the LiDAR system. The light that returns to the LiDAR system will then usually be focused on a photo-diode by a second lens. The photo-diode will produce a small current, which depends on the intensity of the light that hits the photo-diode. This signal is passed through a transimpedance amplifier for further processing. Often, a comparator is used to check whether it passes a certain threshold. If so, a target detection is considered to have taken place and the time is stored. This is then compared with the time the pulse was sent to find the time of flight.

## 2.3. Functions of LiDAR systems

We will now generalise the functions encountered in the simple LiDAR system described in the previous section to extract the more abstract functionalities of LiDAR systems, which will enable us to start defining requirements in the next section. We will only consider standard ranging LiDAR, not doppler LiDAR [9] or imaging LiDAR [27, 59].

### 2.3.1. Channel estimation and target detection

From an abstract view for the simple LiDAR system described in section 2.2, sending out a pulse and checking whether the return signal passes a certain threshold is not one operation, but two. The first is the estimation of the backscatter impulse response of the optical channel, which is the received response after sending out a light pulse. The second is

the detection of an obstacle from this impulse response. This is accomplished by determining whether the estimated backscatter impulse response is larger or higher at a certain location using the comparator.

Though this additional distinction may seem arbitrary, it enables the classification of many LiDAR technologies, as we will show in section 2.5. It also allows convenient mathematical description, as shown in section 2.8.

### 2.3.2. The abstract channel & sample distribution

Until now, we have assumed that an optical channel is given, but in the simple LiDAR system described previously, it is determined by gimballing the LiDAR device such that the optical channel spans different parts of the environment. In a more abstract sense, this is a method to distribute the various distance samples over space. This is required in any 3D LiDAR system, since electrical signals are modelled as 1-dimensional quantities, whilst the environment is a 3-dimensional space. The distribution of measurement samples is thus the problem of splitting the 3-dimensional environment in 1-dimensional channels. The impulse response of the optical channel then becomes a function of the volumetric optical properties of the environment and a steering coefficient vector. It needs to be stressed that this channel need not necessarily be a simple linear trans-section of the environment, but could just as easily be a superposition of these.

### 2.3.3. Towards a Functional Breakdown Structure (FBS)

In summary, measuring the distance to the environment by estimating the optical ToF has three facets:

- representing the 3-dimensional environment in 1-dimensional channels, since only these can be transduced to the inherently scalar electrical signals;
- optical channel estimation, where the backscatter of the channel over distance is estimated;
- target detection, where the location of this target is detected on the basis of the estimated channels.

Channel estimation is an experiment on the channel. This requires the emission of test signal into the channel and the reception of the return signal. Furthermore, like all systems the system needs to interface to a user and needs to preserve itself to be useable. This motivates the FBS in Figure 2.3.

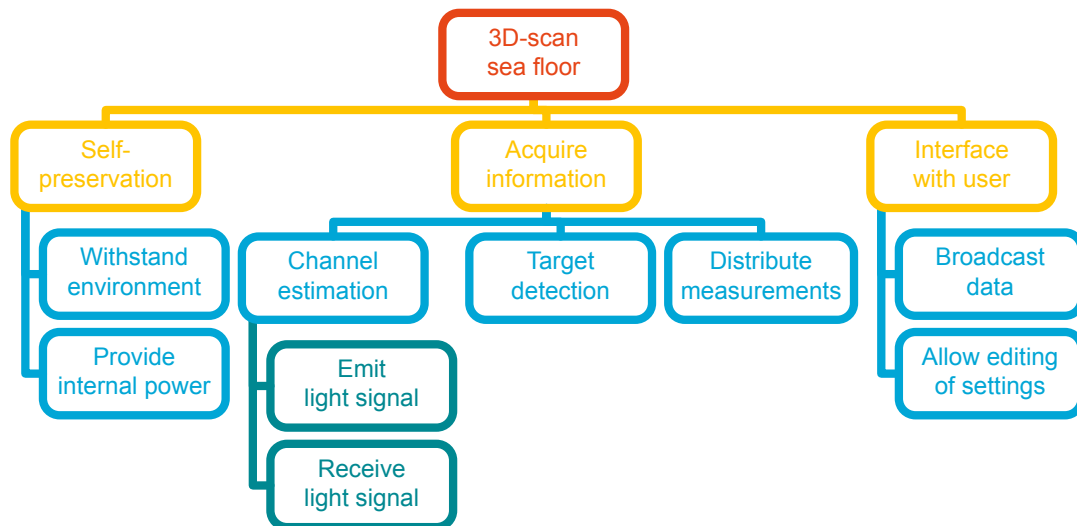


Figure 2.3: LiDAR FBS.

## 2.4. Requirements

### 2.4.1. Towards a Requirement Discovery Tree (RDT)

In order to obtain an exhaustive list of requirements for the system, we constructed a RDT, which will serve as the basis of the upcoming programme of requirements. This entailed finding system-wide performance aspects for each abstract function of the system defined in the FBS discussed in the previous section. The resulting RDT can be found in figure 2.4.

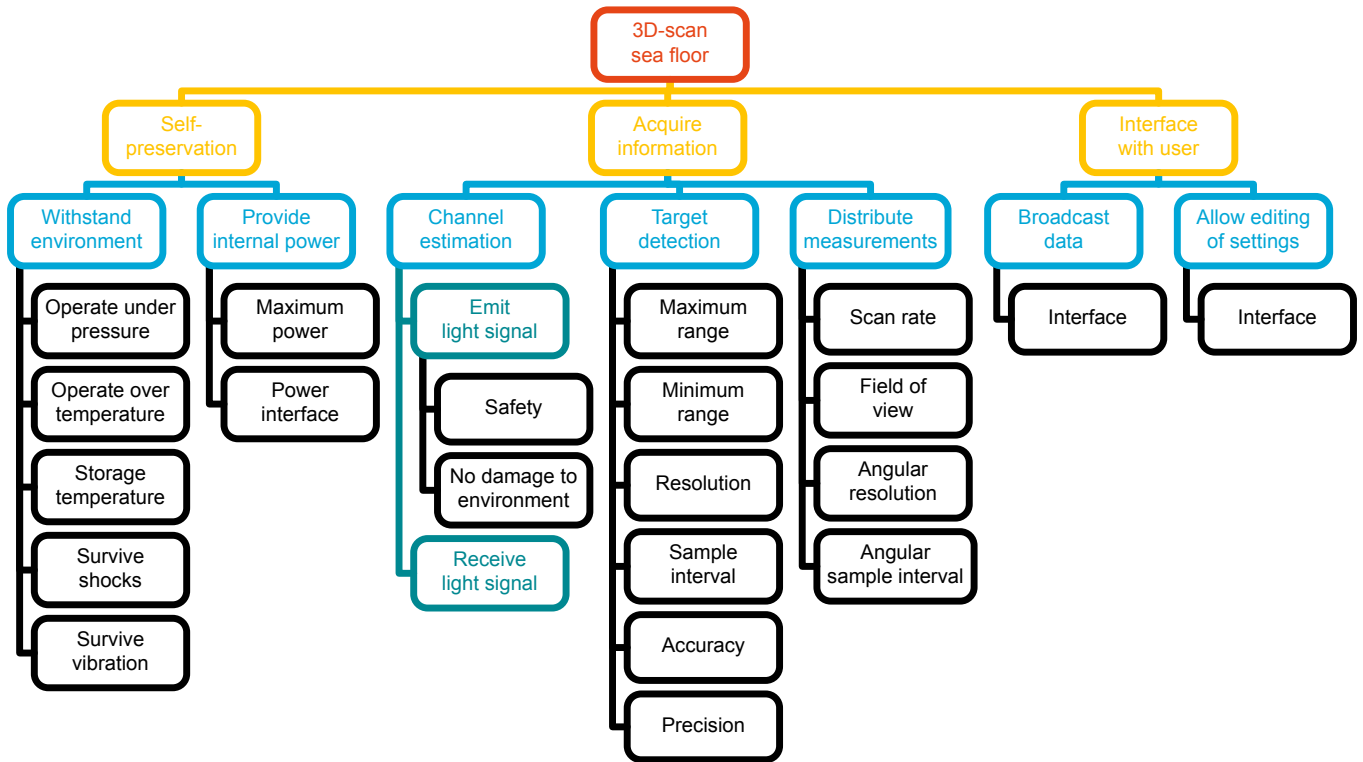


Figure 2.4: SLiDAR RDT.

## 2.4.2. Programme of Requirements

The functions found in the FBS, the requirements found in the RDT and the constraints on the project, form the basis of the program of requirements, which will enable judging of the suitability of design options to form a concept design in later sections. We quantified the requirements based on our market research (part of which is represented in section 2.5) and estimations of the performance required for SLAM. Most of the obligatory requirements were roughly quantified based on an inexpensive triangulating laser scanning system found on entry-level SLAM capable systems, the RPLidar-A1 [76]. The more ambitious goals are based on the unique and high end SL3 underwater LiDAR from 3DAAtDepth [20] and the Velodyne Puck [90], which has been a standard for research into the application of SLAM to self-driving vehicles. Further detailing yielded the programme of requirements on the system shown in table 2.1. We have given each requirement a unique identifier for reference throughout this thesis. We have also given our justification for including the requirement or the value of the requirement for future reference. Finally, we have indicated how the requirement is to be verified as a first step in the creation of verification plans.

Table 2.1: System-wide requirements and justification

ID	Requirement	Verification	Justification
		Test Demonstration Analysis Inspection	
FUN1	The system shall estimate the distance to the environment by measuring the optical time of flight at certain sample points within a certain angular region.	•	Basic functionality of a LiDAR.
FUN2	The system shall be able to stream this measurement data via a serial data protocol.	•	Enables use of the system.
FUN3	All variable parameters should be user-configurable over the serial data protocol.	•	Increases flexibility of the system.
ENV1-a	The system and its internals shall operate in compliance with the requirements up to a pressure of 100 bar.	•	Test limit of MacArtney pressure chamber.
ENV1-b	The system and its internals should operate in compliance with the requirements to a pressure of 600 bar.	•	Test limit of AWI pressure chamber.
ENV2-a	The system shall operate in compliance with the requirements in a temperature range between $-10^{\circ}\text{C}$ and $50^{\circ}\text{C}$ .	•	Minimum and maximum ocean water temperatures, with margin.
ENV2-b	The system shall survive temperatures in a range between $-60^{\circ}\text{C}$ and $70^{\circ}\text{C}$ .	•	Minimum and maximum atmospheric temperatures, with margin.

*Continued on next page*

Table 2.1 – Continued from previous page

ID	Requirement	Verification				Justification
		Test	Demonstration	Analysis	Inspection	
ENV3	The system should survive shocks.	•				In case the robot bumps into obstacles.
ENV4	The system should survive vibrations.	•				To avoid damage from thruster vibrations.
SAF1	The system shall comply with the intent of the IEC60825 safety standard.			•		Ensure team safety.
INF1	The system will receive a 48 V connection.				•	LOBSTER Explorer bus connection.
INF2	The system shall draw no more than 100 W.		•			Sufficiently low power for the LOBSTER Explorer.
INF3-a	The system shall be able to communicate over an Serial Peripheral Interface (SPI) bus.	•				Simple yet high speed and versatile interface.
INF3-b	The system should communicate over a 100BASE-TX Ethernet link or faster.	•				High-speed interface of the LOBSTER Explorer.
PER1-a	The system shall have a maximum range of at least 10 m in 95% transmissive ocean water in a typical ocean environment.	•	•			Braking distance with margin of LOBSTER Explorer.
PER1-b	The system should have a maximum range of at least 40 m in 95% transmissive ocean water in a typical ocean environment.	•	•			Range of commercial systems.
PER2-a	The system shall have a minimum range less than 1 m.	•	•			Braking distance with margin of LOBSTER Explorer.
PER2-b	The system should have a minimum range less than 0.05 m.	•	•			Range of commercial systems.
PER3-a	The system shall have a distance resolution of less than 5 cm.				•	Estimated minimum required for SLAM.
PER3-b	The system should have a distance resolution of 1 mm.				•	Resolution of commercial systems.
PER4-a	The system shall have a distance accuracy of a standard deviation of 5 cm.	•				Estimated minimum required for SLAM.
PER4-b	The system should have a distance accuracy of a standard deviation of 1 mm.	•				Accuracy of commercial systems.
PER5-a	The system shall have a distance precision of 1%.				•	Precision of commercial systems.
PER5-b	The system should have a distance precision of 100 ppm.				•	Estimated minimum required for SLAM.
PER6-a	The system shall have a minimum Field Of View (FOV) of 30° · 30°.				•	Estimated minimum required for SLAM.
PER6-b	The system should have a FOV of 180° · 90°.				•	FOV of commercial systems.
PER7-a	The system shall have a maximum azimuthal sample interval of 1°.				•	Estimated minimum required for SLAM.
PER7-b	The system should have a maximum azimuthal sample interval of 0.1°.				•	Azimuth sample interval of commercial systems.
PER8-a	The system shall have a maximum zenithal sample interval of 15°.				•	Estimated minimum required for SLAM.
PER8-b	The system should have a maximum zenithal sample interval of 0.1°.				•	Zenith sample interval of commercial systems.
PER9-a	The system shall have an angular accuracy better than 1°.	•				Angular accuracy comparable to minimum angular resolution.
PER9-b	The system should have an angular accuracy better than 0.1°.	•				Angular accuracy comparable to maximum angular resolution.
PER10-a	The system shall have an angular precision better than 1°.	•				Angular precision comparable to minimum angular resolution.
PER10-b	The system should have an angular precision better than 0.1°.	•				Angular precision comparable to maximum angular resolution.
PER11-a	The system shall have an maximum update rate of at least 10 Hz.				•	Estimated minimum required for SLAM.
PER11-b	The system should have an maximum update rate of at least 30 Hz.				•	Update rate of commercial systems.
PER13-A	The size of the system shall fit in the mechanical design of the LiDAR				•	As presented by the team of mechanical engineers [65]
PRO1	The project shall be completed by June 21th of 2019.				•	Requirement from BAP.
PRO2	The project shall be documented according to the Electrical Engineering BAP guidelines.				•	Requirement from BAP.
PRO3	The project shall be completed by a team of 6 3rd year bachelor students.				•	Requirement from BAP.
PRO4	The development and fabrication of the electrical system shall cost no more than €3000.				•	Budget.
PRO5	The mechanical scanning stage, optics and embodiment will be developed by a BEP team of mechanical engineers.				•	Agreement with the BEP team of mechanical engineers.

## 2.5. Design options

Having defined the functions of and requirements on our deep sea LiDAR system, this section aims to explore aspects of LiDAR system architectures which fulfil these so that they can be considered as design options for the concept design. To this end, we examine the current state of the art LiDAR techniques along with their merits and weaknesses.

We have organised the techniques by the function they implement to emphasise their commonalities and differences. After considering various solutions for distribution, channel estimation, target detection and digitisation, we summarise these in a DOT for further reflection.

### 2.5.1. Distribution

There are two main approaches to implement the distribution of samples over space:

- scanning systems, where a single measurement beam is rotated over time so that consecutive samples cover different directions;
- concurrent sampling or scannerless systems, where multiple directions are sampled concurrently.

#### Gimballing systems

The advantage of scanning systems is that they make efficient use of the relatively expensive ToF estimation ('laser profiling') hardware. Hence, when LiDAR technology was first developed, only scanning systems were economically feasible. Early scanning systems were mechanical in nature, gimballing the entire laser profiling assembly. The advantage of gimballing is that light beams always enter the receiver from the same angle, simplifying the optical path and ensuring that the effective reception area is constant over any beam deflection  $\phi$ . For these reasons, this method still enjoys widespread use today, primarily in 'spinning LiDARs', which rotate over a single axis. Examples include [58, 90, 75]. There is the disadvantage of requiring connections over one or more rotating axles. This is solved either using slip rings, which are widely considered unreliable and which are unsuited for high-speed data transfer, or using coupled coils for power and optical transmission for data [42], which add complexity.

#### Polygon scanners

Polygon scanners are another mechanical scanning method, where a rotating mirror is used to direct the beam over the FOV [43]. Irregular polygon scanners even enable scanning in the vertical direction by angling each face of the polygon over an axis orthogonal to the rotation direction [43]. These decouple the scanning and laser profiling, but they introduce a Trade-off between the maximum FOV and the amount of vertical samples. They can be used with a separate, fixed reception stage, but this would decrease the effective reception area with  $\cos(\phi)^2$  for samples towards the edges of the FOV. In contrast, it is possible to use the mirror as the return path for the light [38]. In this case, the mirror is at an angle of  $\phi/2$  to the returning light, such that the effective reception area decreases with  $\cos(\phi/2)^2$  towards the edges of the FOV.

#### MEMS micromirrors

MicroElectroMechanical Systems (MEMS) micromirrors are tiny oscillating mirrors used to direct the the beam over the FOV [98]. Their small size is an advantage, though the aperture size and resonant frequency are at odds with each other [48]. They are often driven at resonance to extend the FOV, but when used in liquids, their frequency response is damped such that this is no longer possible and their scan frequency reduces by an order of magnitude from typical 300 Hz to 30 Hz [97, 94].

#### Optical Phased Arrays (OPAs)

With the advent of autonomous driving, manufacturers want to increase the reliability of scanning methods, generating interest in solid-state scanning methods. One of these is the optical phased array, where the beam is composed of a superposition of many smaller beams with tunable phases, resulting in a steerable beam [62]. Advantages include high scan speed, small size and high reliability, but the technology is still in its infancy and thus very expensive, in academia [48] and in industry [57].

## Scannerless versus scanning systems: merits and weaknesses

Thanks to modern advances in miniaturisation, scannerless systems have become viable. The advantage of scannerless systems is that they have a greater scan time per sample, so that the same pulse energy can be achieved using lower peak power illumination. In addition, when limited by eye-safety, longer pulses are permitted higher pulse energies. However, macroscopic mechanical scanning methods and especially spinning LiDARs have the advantage that different pulses are emitted in different positions, such that only a fraction of the total emitted flux flows through an eye-sized area. This means that the pulse energy can be increased [88]. All scanning systems have the advantage of being able to incorporate more refined laser profiling hardware, since cost and effort do not have to be shared over multiple channels but can be focused in a single channel [48].

### Scannerless arrays

Perhaps the simplest is creating an array of differently directed laser profilers operating simultaneously, as demonstrated by Ouster in [60]. They show that laser emitters can be integrated on a single IC using Vertical Cavity Surface Emitting Laser (VCSEL) technology. Advantages include high reliability and low system complexity. Scannerless arrays are often referred to as 'flash multibeam LiDAR'. In this, 'flash' denotes the simultaneous capture of multiple samples, like in a camera sensor illuminated by a flash, and 'multibeam' denotes the multiple targeted beams of light, only illuminating the environment where sampled [60].

### Diffuse source

Instead of replicating directed light sources with each laser profiler in an array, a single diffuse light source can be used [46]. This technique is often referred to as 'flash LiDAR', since multiple samples are captured simultaneously using the same flash of light. Shorter-range systems meant are also referred to as ToF cameras [26]. The advantage is lower system complexity, however much will fall on areas of the environment which are not sampled. Since the total luminous flux flows through a single eye-sized area, the energy of the flash is limited by eye-safety. Then this limits the effective pulse energy at each sample location compared to systems incorporating transmitter arrays.

### Coded aperture

One intriguing possibility is to use Compressed Sensing techniques to reconstruct a scan from samples of a small amount of select beam patterns. A few investigations have been carried out on coded aperture LiDAR [33] and [70]. Both systems send out a diffused source and capture the returned signal with multiple sensors. In comparison with flash LiDAR, less sensors could be used if a static coded aperture is used, this would reduce the cost significantly. Although most literature on compressed sensing does not discuss the effect of noise introduced to the signal before detection, it has been proven that in some cases the signal to noise ratio decreases due to noise folding [5].

## 2.5.2. Channel estimation

The complexity of optical channel estimation techniques is limited due to the required high operating speed. Because of this, only matched filter approaches are commonly implemented and the possible application of modulation is the main difference between these techniques. We will now consider the most common modulations.

### Single pulse

Single pulse LiDAR, or 'pulsed' LiDAR, is perhaps the simplest modulation, and certainly very common in industry [35]. With it, a single pulse high-intensity pulse is emitted each sample [83]. Since the pulse can be modelled as a bandwidth-limited delta pulse, the matched filter is simply a low-pass filter, which is inherent to any input stage. Pulsed illumination can also be easily achieved using a push-pull driver, such that the output stage can be very simple. In short, simplicity is the main advantage of single pulse LiDAR, and it is certainly prevalent in scannerless systems. This simplicity does come at the cost of a relatively large susceptibility to external disturbances. Since all energy is concentrated in a single peak, the pulse energy will be limited by the peak power of the electro-optical transducer, which may be low. Furthermore, at short pulse lengths only low pulse energies are considered to be eye-safe.

## Harmonic

Some time of flight cameras use a harmonic signal<sup>1</sup> for channel estimation. In this case, the time of flight is calculated from a relatively simple phase shift measurement [37]. The advantage is that the usual complexities of high speed ToF estimation can be avoided, since only low-speed amplitude measurements are required. However, usually a harmonic signal would not even be considered for channel estimation. This because due to the tiny bandwidth, all objects in the channel will alias on top of each other. Thankfully, objects farther away in the channel generate weaker returns due to  $R^{-2}$  spreading. Combined with the small spot enabled by the optical extremely high frequencies exploited by LiDAR this makes the nearest return dominant, which is usually the only return of interest. However, it is impossible to distinguish a dominant return from a dominant return at a length  $c \cdot f/2$  further away, since both alias to the same point. Hence, the domain of harmonic channel estimators is usually limited to  $[0, \cdot f/2)$  in order to prevent these range ambiguities. Though this limit could be overcome by using a select few frequencies, any amount of near-field volumetric backscatter due to the environment could become the dominant return at longer ranges due to higher  $R^{-2}$  spreading. Hence, harmonic channel estimation is usually reserved for short range indoor use in time of flight cameras.

## FMCW

Frequency Modulated Continuous Wave (FMCW) systems continuously transmit a frequency modulated light wave. This modulation enables a Continuous Wave system to be used for distance measurements. The distance measurement for FMCW is done by comparing the received signal with a reference signal [39]. The distance between the source and the reflecting object can be calculated as  $R = c_0 |\Delta t|/2$ . Here  $\Delta t$  is the measured delay time between the reference and the received signal. An inherently high SNR makes this technique advantageous. A disadvantage is the need of high bandwidth to increase the maximum ranging distance, and the need for a heterodyne receiver.

## Pulse trains

In pulse train implementations, multiple pulses are sent for every distance sample. The received signals are then averaged for higher Signal to Noise Ratios (SNRs). Correlation processing is then used to find the ToF [34]. The advantage of a pulse train is that the total pulse energy is spread over many pulses with an equivalent bandwidth, such that the peak power can be reduced. The downside is that in low SNR regimes, the nonlinearity of detection methods cause noise standard deviation after detection to grow superlinearly as a function of noise standard deviation before detection. Because of this, the pulses must be averaged before detection. This either requires expensive full digitisation of the amplitude of the pulses or complex analog filters.

### 2.5.3. Target detection

As with channel estimation, the complexity of optical channel estimation techniques is limited due to the required high operating speed. We will now consider the most common techniques.

#### Static thresholding

The simplest technique is static thresholding, where the return signal is compared to a constant threshold [83]. A target detection is recorded when the signal passes this threshold. The advantage is the simplicity, but the disadvantage is that the method is unreliable in the presence of volumetric backscatter. In that case, backscatter from scattering media close-by will be brighter than returns from faraway legitimate targets, due to the attenuation of light over distance. In air, this usually is not a problem, since it is a near-perfect medium. However, bad weather such as mist can interfere with this detection method [95].

#### Adaptive thresholding

The susceptibility of static thresholding implementations to volumetric backscatter can be overcome by adapting the threshold over time or based on the returned signal. Examples include Constant False Alarm Rate (CFAR) detectors, which adapt the threshold according to a function of the background surrounding the sample and also more complex Bayesian methods [56]. The main advantage is lower susceptibility to volumetric backscatter, but the approaches

---

<sup>1</sup>A square is often used for simplicity, but the input signal is typically thresholded, such that the square wave can be regarded as the binary equivalent of a sine wave.

are noncausal and may require sophisticated processing (Bayesian methods). This either requires expensive full digitisation or complex analog filtering.

#### 2.5.4. Digitisation

The incoming light is converted to an analog electrical signal, but most LiDAR systems provide their ToF estimates digitally. Hence the signal must be digitised in order for the digital part of the system to properly process the information. Different types of digitisation techniques were considered for the design of the LiDAR and will be discussed in the forthcoming sections.

##### Analog to Digital Converter (ADC)

An ADC (as the name entails) fully converts the analog signal to a proper digital signal. They are often used in systems which fully digitise the light intensity signal. An advantage of ADC based implementations is the lower analog complexity, as complex signal processing can be implemented in software. Another advantage of an ADC implementation is the potential of acquiring volumetric density information about the 3D space, which could be of interest to the user. However, due to the high bandwidth required for LiDAR applications, sufficiently capable ADCs tend to be expensive. Also, the dynamic range of these high-speed ADCs is often insufficient for LiDAR applications, so the input dynamic range must be compressed using either nonlinear circuits [8] or time-variant amplifiers [3].

##### Time to Digital Converter (TDC)

Time to Digital Converter (TDC) is a device which reads out a digitised time interval between two rising edges [12]. Advantage of a TDC are the conceptual simplicity and low cost. The disadvantage is that a TDC based implementation forces signal processing to be implemented in analog electronics, increasing complexity. Another disadvantage is that the output data is only the distance to a target and thus no other information about the channel can be acquired such as target strength or multiple returns.

##### Phase measurement

In phase measurement digitisation, the time of flight is found by comparing the accumulated electrical of the normalised received pulse while the system was transmitting  $Q_1$  and the accumulated normalised received electrical charge while the system is not transmitting  $Q_2$ . From these, the distance is calculated using equation 2.1.

$$d = 0.5 \cdot c \cdot \Delta t \cdot \left( \frac{Q_1}{Q_1 + Q_2} \right) \quad (2.1)$$

The advantage of this method is the simplicity, and it is often used in ToF cameras [37]. The major disadvantage is the susceptibility to volumetric backscatter. The returned pulse is required to be either fully on or fully off for processing, which entails thresholding. However this threshold is difficult to define in the presence of volumetric backscatter, as explained previously.

#### 2.5.5. Design Option Tree (DOT)

We will now present a short visual summary of the high-level design options for LiDAR systems discussed so far in the DOT shown in figure 2.5. This will serve as an accessible reference for the upcoming concept selection.

### 2.6. Concept selection

In this section, all of the discussed design concepts for each part of the LiDAR system are weighed in upon. Given the criteria for each part, a decision is then made as to which design concept is most suitable for each part of the LiDAR. In the forthcoming sections, the decision for each part of the LiDAR is discussed.

#### 2.6.1. Distribution

Table 2.2 illustrates the advantages of the different distribution methods. Based on the criteria given in the table, it was decided to implement a polygon scanner for the distribution system, since we only considered its implementation to be time feasible.

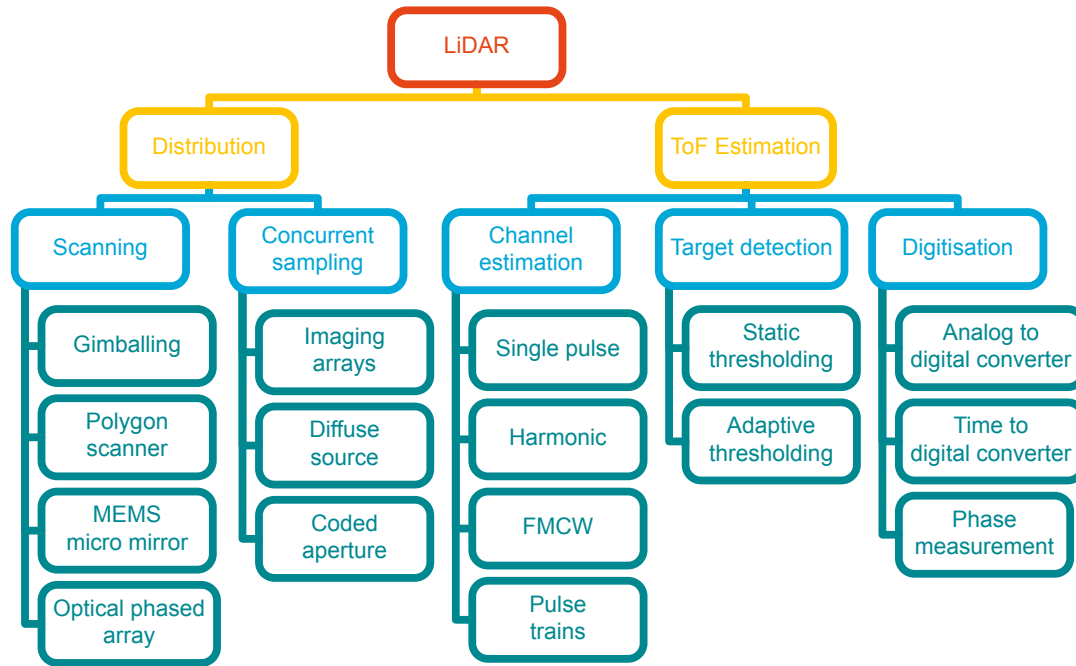


Figure 2.5: High-level LiDAR DOT.

Table 2.2: Trade-off table for the distribution

	Distribution							Explanation
	Gimball	Polygon	MEMS	OPA	Array	Diffuse	Coded	
Size	±	-	+	+	+	+	±	Size should comply to requirement PER13-A
Fluid Function	±	±	-	±	+	+	-	The system will be fluid-filled as per ENV1-a and ENV1-b
Implementation time	±	+	±	-	±	±	-	Development time is limited, as per PRO1

### 2.6.2. Channel estimation

Table illustrates 2.3 channel estimation trade-offs. We decided to use the single pulse technique based on since it had the best feasibility per PRO1 and PRO3 at an acceptable range to satisfy PER1-a and PER1-b.

Table 2.3: Trade-off table for the channel estimation method

	Channel estimation				Explanation
	Single	Harmonic	FMCW	Pulse train	
Modulation	+	+	-	±	Simplicity of the modulation technique
Detection	+	±	-	±	Complexity of the detection method
Range	±	-	+	+	Maximum range that can be achieved

### 2.6.3. Digitisation method

For the digitisation method, it is of utmost importance to minimise the noise in the received signal and implementation complexity. For the options that were considered for the LiDAR, it is important to discuss the quality of information versus the complexity of the implementation. Table 2.4 illustrates the advantages for each digitisation method. In order to maintain feasibility as per PRO1 and PRO3 at the decision was made to implement a TDC for the digitisation since it can be validated the quickest.

Table 2.4: Trade-off table for the digitisation technique

	Digitisation			Explanation
	ADC	TDC	Phase	
Complexity	+	-	-	Complexity of the implementation
Flexibility	+	-	-	Flexibility of the implementation with the other devices
Time to prototype	-	+	-	Time to first test of the simplest iteration

## 2.6.4. Target detection

When choosing a target detection technique it is of importance to keep in mind that the operating environment is sea water. The trade-offs between static and adaptive target detection can be found in table 2.5. Though the adaptive target detection is very complex, its resilience against backscatter is of the utmost importance. Since static detection would give too many spurious detections to meet PER9-a and PER9-b, it was decided to implement adaptive detection, despite the additional complexity, possibly interfering with PRO1 and PRO3.

Table 2.5: Trade-off table for the target detection techniques

	Target detection		Explanation
	Static	Adaptive	
Complexity	+	-	Complexity of the implementation
Flexibility	+	+	Flexibility of the implementation with the other devices
Reliability	-	+	Reliability in the presence of close-by scattering media

## 2.7. Subsystem selection

As described in the overview of a simple LiDAR in section 2, a transmit stage consisting of a laser diode together with a laser driver are necessary to convert an arbitrary timing signal to a laser pulse that leaves the system. Also, a receiving stage consisting of a photo diode, together with the necessary data processing was needed to in fact retrieve the light and process the data. The focusing of the beam is not considered in the scope of the electrical part of the SLiDAR because this is mainly a mechanical issue. The system described in section 2 does not have any form of beam steering and can thus only measure one point. However, the SLiDAR has to measure multiple points in space, thus some sort of beam steering has to be implemented. Furthermore, The data has to be processed and all actions, such as choosing a point in space to measure the distance or sending out a laser pulse, have to be coordinated. This is why we came to the following subsystem division.

- A transmitting stage
- A receiving stage
- A beam Steering stage
- A Data processing stage

## 2.8. System modelling

The subsystem division generates requirements on the interfaces of subsystems. Two important interfaces is the interface of the transmission stage to the optical channel and the channel to the reception stage. These take the form of the optical output power of the transmission stage, the input sensitivity and input referred noise of the reception stage, the wavelength and the bandwidth of both subsystems. Together, these determine the minimum range, maximum range and distance resolution. In order to dimension these subsystem requirements, their relation to the system requirements needs to be found. In this section, we construct a simplified model of the optical channel to find this relation.

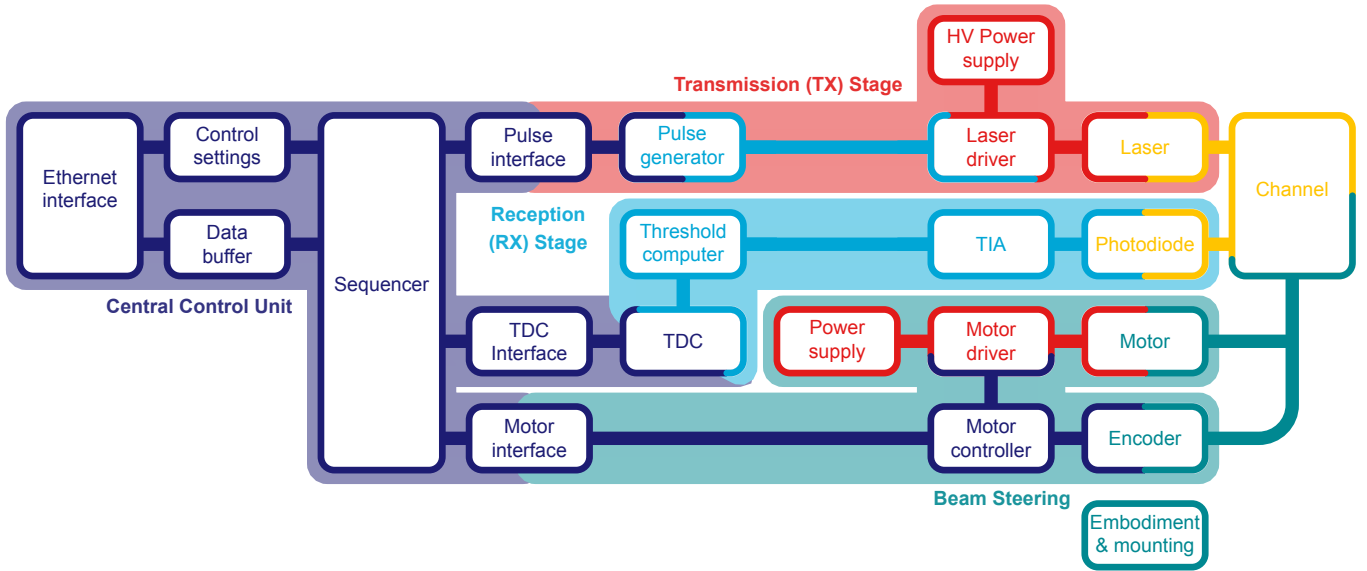


Figure 2.6: Low-level system architecture. Digital is purple, analog signal processing is cyan, high power is red, optical is yellow and mechanical is green. Modules converting domains are a mix of colours.

### 2.8.1. Towards a simple model

We have defined a LiDAR device as an apparatus which measures the distance to objects by estimating the optical time of flight to those objects. Then a LiDAR device detects features of its environment. We model the environment as two scalar fields:

- A transmissivity field  $T(\vec{R})$ , which models the amount of light which is not absorbed or reflected when a beam travels through a medium, such that the forward intensity  $\lim_{\Delta\ell \rightarrow 0} I(\vec{R} + \Delta\vec{\ell}) = I(\vec{R}) \cdot T^{|\Delta\vec{\ell}|}$ . It must always have a value between 0 and 1, since we assume that there are no energy sources to amplify the light in the environment.
- A reflectivity field  $\beta(\vec{R})$ , which models the amount of light reflected back at the source at each point, such that the magnitude of the backscattered light is  $I_b = I \cdot (1 - T) \cdot \beta$ . It must also always have a value between 0 and 1.

LiDAR devices can detect only these fields. This is accomplished by characterising one or a variety of optical paths through the medium and applying channel estimation techniques. Other models model the scattering of the beam in space using distribution function [47]. Assuming that multiple backscatter effects are insignificant and using the fact that our system has a coaxial receiver and transmitter, only the amount of light propagating to the next distance segment needs to be considered, and the simplified model suffices.

Sometimes knowledge of these scalar fields is enough. Cloud observations would be complete with complete knowledge of these scalar fields. In other cases, distances to interesting objects must be inferred from these fields. In SLAM applications, one is interested in solid obstacles. Most are characterised by  $T \approx 0^2$ .

Then LiDAR devices must do two things:

- Channel estimation
- Obstacle detection

To constrain the key system parameters, We will now model the channel and the optical signal therein in the context of obstacle detection.

### 2.8.2. Channel impulse response

For a perfectly collimated beam travelling between points  $\vec{a}$  and  $\vec{b}$  the intensity  $I$ :

$$I(\vec{b}) = I(\vec{a}) \cdot \exp\left(\int_{\vec{a}}^{\vec{b}} \ln(T(\vec{R})) \cdot |d\vec{R}|\right)^2 \quad (2.2)$$

<sup>2</sup>Glass is an exception, but it is rare in underwater LiDAR applications

We define the magnitude of light reflected back at each position as:

$$I_b(\vec{R}) = I(\vec{R}) \cdot (1 - T(\vec{R})) \cdot \beta(\vec{R}) \quad (2.3)$$

Incorporating  $x^2$  spreading back from the target to the receiver for large  $x$ , modelling optical inefficiencies using a factor  $\eta$ , assuming lambertian reflection and assuming that the full beam is reflected we find for the impulse response in terms of power:

$$p(x) = \eta \cdot \exp\left(\int_0^{x/2} \ln(T(\tau)) d\tau\right)^2 \cdot (1 - T(x/2)) \cdot \beta(x/2) \cdot \frac{A_0}{(x/2)^2} \quad (2.4)$$

In which  $x = u_p \cdot t$ ,  $A_0$  is the effective receiver area.

### 2.8.3. Towards wavelength requirements

At longer distances, the exponential term in equation 2.4 modelling bulk absorption will start to play a dominant role. The absorption is highly dependent on the wavelength. Hence, a wavelength should be selected such that absorption is minimised. The absorption in different types of sea water is very well classified by Jerlov's water mass classification [49]. This shows that absorption is maximised for a wavelength around 520 nm in type I, II and III oceanic waters. Traditionally, this wavelength would be avoided due to the significant solar irradiance causing interference, but this light does not penetrate to the deep sea. We have detailed this consideration as requirement TX-PER1 in table 2.6.

### 2.8.4. Towards power & input sensitivity requirements

In order to find the required power and input sensitivity, we modelled a maximally absorptive homogeneous channel using  $T = 95\%$  as per PER1-a and PER1-b. We assume that volumetric backscatter is caused by floating particulates of the same material as sediments covering the sea floor, such that  $\beta(x) = \beta$  is everywhere constant at a minimum value of 0.1 based the darkest sediments in underwater reflectance measurements in [96].

A main factor in the attenuation of the transmitted signal, are the optical elements. Firstly lenses always have a small inefficiency, this has to be taken into account. Secondly, focusing the outgoing laser light on the photo detector also greatly influences the received optical power. The mechanical design therefore already introduces some losses in the optical path.

We implemented a Matlab script with our model to find the range associated with input threshold and output power values. We used values given in the reference design [83] as a basis for the the parameters and adjusted to find a reasonable division of requirements, given in table 2.6. The Matlab script can be found in A.1.

### 2.8.5. Towards bandwidth requirements

The bandwidth is directly related to the outgoing pulse width, so determining the pulse width fully constrains the bandwidth. We will now investigate the effects of changing the pulse width on the channel estimate to find the required pulse width.

In general range finding, the pulse width determines the distance resolution of the system. If objects are closer to each other than the pulse width, they become indistinguishable. Because of the small beam diameters of LiDAR systems, the assumption is often made that all light is reflected by a singular target, such that there is only a single return. However, the backscatter also generates weak returns. Since these returns are distributed over space, the signals ranging between those on the front of the pulse reflected from farther away and the signals on the back of the pulse reflected from shorter away will reach the receiver simultaneously. This generates interference, which scales with pulse width and must be limited. We will now use our simplified model to express this interference in terms of the pulse width of the subsystems to constrain the pulse width.

To find estimate the maximum interference versus distance, we assume clear water before that distance and the most absorptive water thereafter. To simplify calculations, we also ignore the absorption within the length of the channel occupied by the pulse, which will lead to slight overestimation. We can then remove the exponential term from equation 2.4 and correlate with a square pulse to find the maximum interference versus distance in equation 2.5.

$$p_i(x) = 4\eta\beta A_0 \cdot (1 - T_{min}) \cdot \left(\frac{1}{x-L} - \frac{1}{x}\right) \quad (2.5)$$

Any detector should not register a detection at this maximum interference level. This puts a lower limit on the threshold. We can express this by modelling the maximum factor  $\alpha$  that the threshold can be lower to maximum return. This

is obtained when  $T = 0$  after clearwater, such that bulk absorption can be ignored. This yields equation 2.6 for  $x > L$ .

$$p_{max}(x) = 4\eta\beta A_0 \cdot \frac{1}{x^2} \quad (2.6)$$

Since  $p_i(x)$  falls superquadratically for  $x \rightarrow \infty$ , there is a range where  $p_i(x_{min}) = p_{max}(x_{min})/\alpha$ . Below this range, it can not be guaranteed whether an obstacle is detected or volumetric backscatter. Solving the equation yields equation 2.7.

$$L = \frac{x_{min}}{(\alpha \cdot (1 - T_{min}) \cdot x_{min} + 1)} \quad (2.7)$$

We assume that  $\alpha = 6$  is a reasonable value,  $T_{min} = 0.8$ , and  $x_{min} = 1$  m per PER2-a or  $x_{min} = 0.05$  m per PER2-b. This gives a pulse width  $L = 0.45$  m per PER2-a, which corresponds to 2 ns and a pulse width of  $L = 0.05$  m per 0.2 ns PER2-b. This corresponds with bandwidths of 0.5 GHz and 5 GHz respectively. These requirements are detailed in table 2.6.

Table 2.6: Subsystem requirements

ID	Requirement	Verification				
		Test	Demonstration	Analysis	Inspection	
TX-PER1	Light emitted by the transmission stage shall have a wavelength between 505 and 535 nm .	•				Minimises absorbance while allowing slight deviations due to changing operating conditions.
TX-PER2	The optical power emitted by the transmission stage shall have a value higher than 6 W	•				In order to meet the range specifications.
TX-PER3a	The pulse width of the light emitted by the transmission should remain smaller than 2 ns	•				In order to limit the interference.
TX-PER3b	The pulse width of the light emitted by the transmission should remain smaller than 0.2 ns	•				In order to limit the interference.
RX-PER1	The threshold of the RX stage shall be less than 0.05 W.	•				In order to detect at the required range.
RX-PER2a	The bandwidth of the RX stage shall be at least 500 MHz	•				In order to limit the interference.
RX-PER2b	The bandwidth of the RX stage should be at least 5 GHz	•				In order to limit the interference.

## 2.9. Functional Overview

This section serves as a brief overview of the functional operation flow of the proposed LiDAR design from section 2.7. From this overview, the interfaces between subsystems are defined. The reader can use this section to put the design of the subsystems in following chapters into the perspective of the LiDAR system as a whole.

### 2.9.1. Functional flow

A high-level functional overview of a single distance measurement of the proposed LiDAR design is given in figure 2.7. The motor in the diagram rotates the polygon mirror. The direction in which the laser pulse is sent depends on the angular position of this mirror. The angular position is most accurately known when the mirror rotates with a steady-state angular velocity. Hence, the CCU waits for steady-state motor rotation before measurements start.

A distance measurement consists of a number of sequential events. The CCU instructs the Transmission (TX) Stage to send a laser pulse to the measurement channel. The timestamp of this event is recorded by the TDC. A laser reflection comes back from the channel, and is detected by the APD. The Reception (RX) stage converts this detection to a pulse, of which the TDC records the timestamp. The CCU computes a distance estimate from the two TDC timestamps, and streams it to the user via a serial data protocol.

Laser pulses are transmitted in packets called frames. The relation between the timing of frame transmission and the rotation of the mirror is illustrated in figure 2.8. When the line of sight of the laser diode crosses a corner of the mirror, the Beam Steering system will detect this as an FOV-corner event. When this detected corner marks the start of the FOV, it is called an FOV-start event. The CCU uses these events to time the laser pulse transmission of the Transmission Stage. The red areas in the figure indicate dead zones. These are margins within which the laser might hit a mirror corner, which would make the measurement invalid. The CCU will not send.

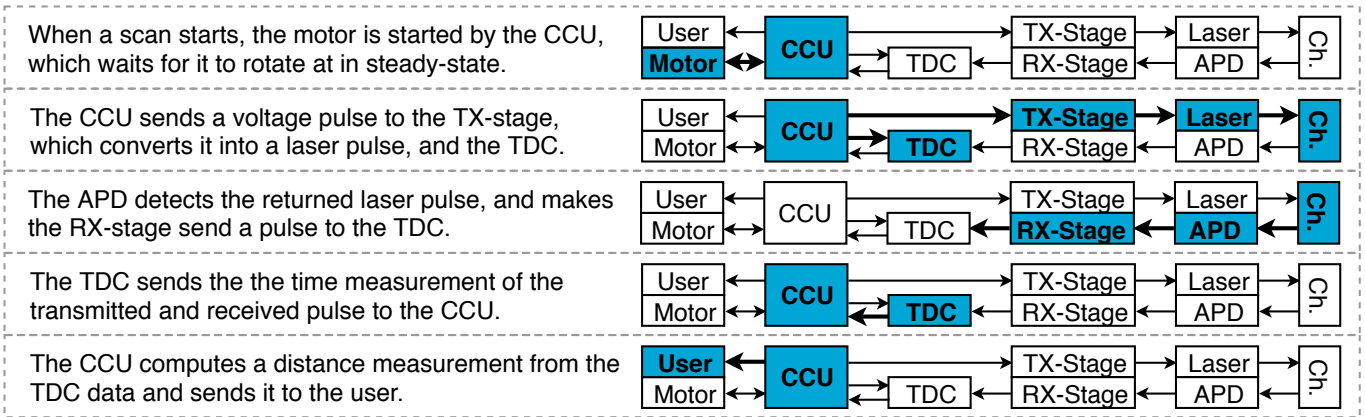


Figure 2.7: High-level functional overview of a single distance measurement. Active parts of the system during a step are highlighted.

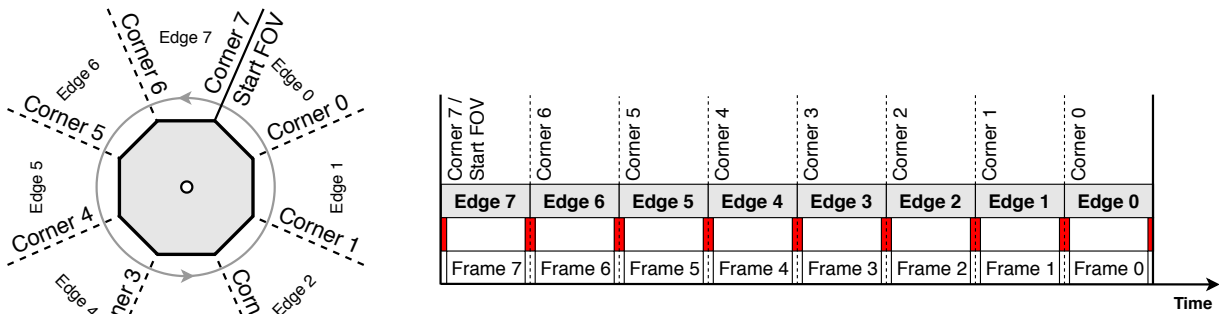


Figure 2.8: Illustration of the correspondence between polygon mirror rotation and pulse timing.

### 2.9.2. Interface specification

The high-level functional overview of each subsystem (see figure 2.6) can be derived from the discussion in section 2.9. Table 2.7 shows the data flow between subsystems. This table assumes the use of the AS6501 TDC IC.

Table 2.7: Data flow between subsystems from figure ??.

<b>From:</b>	<b>To: CCU</b>	<b>Transm. Stage</b>	<b>Reception Stage</b>	<b>Beam Steering</b>
<b>CCU</b>	None	<ul style="list-style-type: none"> <li>• Pulse frames</li> <li>• Reference signals for the laser driver</li> </ul>	<ul style="list-style-type: none"> <li>• Control signals for the threshold computer</li> <li>• Oscillator to aid in generation of bias signal for the APD</li> <li>• Configuration and reference signals for the TDC</li> <li>• Pulse frame triggers</li> </ul>	<ul style="list-style-type: none"> <li>• Motor start and stop signals</li> </ul>
<b>Transm. Stage</b>	<ul style="list-style-type: none"> <li>• Serial LVDS TDC timestamp data (2 channels)</li> </ul>	None	None	None
<b>Beam Steering</b>	<ul style="list-style-type: none"> <li>• Indication if motor rotates in steady-state</li> <li>• FOV-start and FOV-corner event detections</li> </ul>	None	None	None



## Program of requirements

The requirements for the LiDAR system have been setup in the previous chapter and are presented in table 3.1. Some extra requirements were derived in a later section. Not all of these requirements are related to this specific thesis, this chapter will present the requirements most important for the thesis. Here after some new requirements were derived, this derivation will also shortly be discussed.

Table 3.1: System-wide requirements and justification

ID	Requirement	Verification				Justification
		Test	Demonstration	Analysis	Inspection	
ENV1-a	The system and its internals shall operate in compliance with the requirements up to a pressure of 100 bar.	•				Test limit of MacArtney pressure chamber.
ENV1-b	The system and its internals should operate in compliance with the requirements to a pressure of 600 bar.	•				Test limit of AWI pressure chamber.
ENV2-a	The system shall operate in compliance with the requirements in a temperature range between $-10^{\circ}\text{C}$ and $50^{\circ}\text{C}$ .		•			Minimum and maximum ocean water temperatures, with margin.
ENV2-b	The system shall survive temperatures in a range between $-60^{\circ}\text{C}$ and $70^{\circ}\text{C}$ .		•			Minimum and maximum atmospheric temperatures, with margin.
ENV3	The system should survive shocks.	•				In case the robot bumps into obstacles.
ENV4	The system should survive vibrations.	•				To avoid damage from thruster vibrations.
SAF1	The system shall comply with the intent of the IEC60825 safety standard.		•			We like both our eyes being functional.
INF1	The system will receive a48 V connection.			•		LOBSTER Explorer bus connection.
PER1-a	The system shall have a maximum range of 10 m in type 3 ocean water in a typical ocean environment.	•	•			Braking distance with margin of LOBSTER Explorer.
PER1-b	The system should have a maximum range of 40 m in type 3 ocean water in a typical ocean environment.	•	•			Range of commercial systems.
PER2-a	The system shall have a minimum range less than 1 m.	•	•			Braking distance with margin of LOBSTER Explorer.
PER2-b	The system should have a minimum range less than 0.05 m.	•	•			Range of commercial systems.
PER5-a	The system shall have a minimum FOV of $30^{\circ} \cdot 30^{\circ}$ .			•		Estimated minimum required for SLAM.
PER5-b	The system should have a FOV of $180^{\circ} \cdot 90^{\circ}$ .			•		FOV of commercial systems.
PER6-a	The system shall have an azimuth angular resolution of $1^{\circ}$ .			•		Estimated minimum required for SLAM.
PER6-b	The system should have an azimuth angular resolution of $0.1^{\circ}$ .			•		Azimuth resolution of commercial systems.
PER7-a	The system shall have a zenith angular resolution of $15^{\circ}$ .			•		Estimated minimum required for SLAM.
PER7-b	The system should have a zenith angular resolution of $0.1^{\circ}$ .			•		Zenith resolution of commercial systems.
PER10-a	The system shall have a maximum update rate of at least 10 Hz.			•		Estimated minimum required for SLAM.
PER10-b	The system should have a maximum update rate of at least 60 Hz.			•		Update rate of commercial systems.
TX-PER2	The optical power emitted by the transmission stage shall have a value higher than 6 W	•				In order to meet the range specifications.
TX-PER3	The pulse width of the light emitted by the transmission should remain between 2 ns and	•				In order to limit the interference.
TX-PER1	Light emitted by the transmission stage shall have a wavelength between 505 and 535 nm .	•				Minimises absorbance while allowing slight deviations due to changing operating conditions, section 2.8.
PER13-A	The Printed Circuit Board (PCB) size of the system shall fit in the mechanical design of the LiDAR		•			As presented by the team of mechanical engineers [65]

*Continued on next page*

Table 3.1 – Continued from previous page

ID	Requirement	Verification				Justification
		Test	Demonstration	Analysis	Inspection	
PER14-A	The system shall create pulses with a repetition rate of at least 21.6 kHz	•	•			Derived from the polygon mirror specifications as given in the Appendix
PER14-B	The system should create pulses with a repetition rate of at least 98 MHz			•		Derived from previous requirements as given in the Appendix
PER15	The APD bias shall supply the photodiode of the receiving stage with a voltage of 130 V.	•				Derived from the system requirements of the receiving stage
PER16	The system shall be exposed to either of three liquids, IPA, Mineral oil or FC-770	•				Based on the mechanical design.
PER17	The system shall receive the necessary digital signals from an FPGA board	•				The FPGA was selected by the receiving stage.
PRO1	The project shall be completed by June 21th of 2019.				•	Requirement from BAP.
PRO2	The project shall be documented according to the Electrical Engineering BAP guidelines.				•	Requirement from BAP.
PRO3	The project shall be completed by a team of 6 3rd year bachelor students.				•	Requirement from BAP.
PRO4	The development and fabrication of the electrical system shall cost no more than €3000.				•	Budget.
PRO5	The mechanical scanning stage, optics and embodiment will be developed by a BEP team of mechanical engineers.				•	Agreement with the BEP team of mechanical engineers.

# 4

## Design of TX stage

In this chapter, the overall design for the transmission stage is thoroughly discussed and documented. Each part of the design of the transmission stage is presented with multiple design methods and concepts, these ideas will then be discussed and weighed in on the advantages and disadvantages of each idea. After that a decision is made as to which idea is most suitable to each part of the transmission stage and the overall design of the transmission stage is given at the end of the section.

### 4.1. Light element

In this section, all of the design considerations for the optical medium for the transmission stage are thoroughly discussed and documented. The main points of interest for choosing the most suitable optical medium is that the optical signal should be **the colour green** and should have **high optical output power**, this was discussed previously in section 3.

#### 4.1.1. Laser vs LED

The first step in the design process of the transmit stage is to determine the light source. This could either be implemented using a LED or a laser. The main advantages and disadvantage of each source were researched and are given in table 4.1, this table is based on [31]. The conclusion was drawn that due to the beam divergence, more information can be found in the Appendix A.4, and coherence of the laser, it would be easier to focus a laser beam. Therefore it was decided to implement a laser as the optical medium for the transmission stage of the LiDAR.

Table 4.1: LED versus Laser

Light element	Advantages	Disadvantages
LED	-Low cost -Pressure tolerant	-Incoherent light -Spontaneous emission -Nonlinear output characteristic -Large beam divergence
Laser	-Linear output characteristic -Stimulated emission -Coherent light -Small beam divergence	-High intensity, not eye-safe -Higher cost

#### 4.1.2. Laser types

With the decision made to go forth with a laser in the transmission stage of the LiDAR, the next step is to choose which laser type is most suitable for the transmission stage and also adheres to the set requirements. Many laser types were taken into consideration, a brief explanation of each laser type is given as follows:

- Gas laser  
A laser in which current is discharged through a gas, this will then produce a laser beam.
- Semiconductor laser  
This laser type is very similar to the solid state laser as the laser medium is also solid, yet the distinction is made

that the solid medium is made of a semiconductor material.

- Liquid laser  
Laser type in which a laser beam is produced by discharging current through a liquid.
- Fiber laser  
This laser type comprises an optically doped fiber gain medium, discharging current through the medium will induce a high quality laser beam

A more elaborate explanation of each of these laser types can be studied in Appendix A.5 with all of the advantages and disadvantages discussed. Knowing this type of information of each laser type, the next step is to check the availability and cost of these types of lasers. This narrowed the search down to only semiconductor lasers, better known as laser diodes.

### 4.1.3. Semiconductor laser

After the decision was made to use a laser diode as the optical element of the transmission stage, the next step was to choose which laser diode in the market is the most suitable for the design. There are some key points that were taken into consideration when choosing the right laser diode and they are listed as follows.

1. Peak optical output power  
The laser diode should be able to produce a laser beam at a high enough power level
2. Beam divergence  
The beam divergence of the laser diode should not be too high, or else the complexity to collimate the laser beam will increase. The study of beam divergence is briefly discussed in appendix A.4.
3. Wavelength of the laser diode  
The laser diode should of course emit a laser beam at a wavelength that is equivalent to that of the colour green on the electromagnetic wave spectrum. This wavelength should be around 520 nm, as discussed in section 3.

The Commercial Off-The-Shelf (COTS) laser diodes with a wavelength of around 520 nm usually have very low optical power, this is a phenomena known as the green gap problem [51]. Green laser pointers however are able to produce more optical output power. The trick with laser pointers is that it actually consists of an infrared semiconductor laser in combination with a frequency doubling crystal, as given in Figure 4.1.

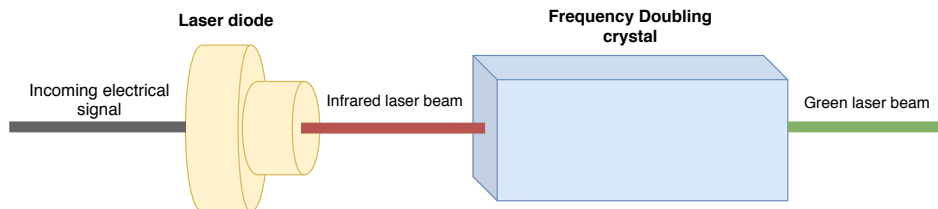


Figure 4.1: Figure depicting the topology of the laser diode in conjunction with a frequency doubling crystal

### 4.1.4. Frequency doubling crystal

To further understand the topology, the concept as to how a frequency doubling crystal functions must first be understood. The explanation for the frequency doubling crystal is given in appendix A.4. The main idea is to implement a laser with a higher wavelength and presumably a higher optical power in conjunction with the frequency doubling crystal, this in order to yield a higher optical power. As the name already entails, the said crystal will double the frequency of the incoming optical signal, thus the output will have a wavelength which is half of the wavelength of the incoming signal. The main issues with implementing said crystal is the **cost**, **efficiency**, **dependency on temperature** and **complexity**. For these reasons, it was decided not to implement such crystal, yet the idea remains fruitful.

## 4.2. Optical Amplifier

The implementation of a sole laser diode begs the question of whether or not this would have enough optical output power to reach the set range requirement. In electronics, the main method used to increase the power level of a signal is to use an amplifier. Likewise, in the area of laser technology such an amplifier exists to amplify the optical output power of a laser and this type of amplifier is called an optical amplifier. The optical amplifier amplifies the optical signal without first converting the signal to an electrical signal, which further increases interest for usage within the system.

There were some types of optical amplifiers that were considered for the design of the transmission stage and they are briefed upon as follow.

- Semiconductor optical amplifier
- Erbium Doped Fiber Amplifier
- Tapered amplifier
- Solid state amplifier

A more in depth explanation of each amplifier is given in Appendix A.6 with the disadvantages and advantages of each amplifier analysed. While the prospect of using an optical amplifier is very alluring, it does unfortunately adds more complexity to the overall system. It was therefore decided to not implement such an amplifier within the LiDAR system.

### 4.3. Laser driver

As previously mentioned, in section 2.8, the goal is to keep the laser pulsing with the smallest pulse width in order to have less interference. Furthermore in order to meet the range requirements the optical pulse peak power of the laser diode must be as large as possible. This peak power is, namely related to the average power of the laser diode, the repetition frequency and the pulse width by the following equation 4.1.

$$P_{peak} = \frac{P_{avg} * T_{rep}}{T_{pulse}} \tag{4.1}$$

Here  $P_{avg}$  is the optical output power of a laser diode operating in continues wave mode, which is a given maximum value. The  $T_{rep}$  is the repetition rate of the pulses and  $T_{pulse}$  is the pulse width. This relation clearly shows that a smaller pulse width also increases the peak pulse power of optical pulse, which gives another reason for keeping the pulse width as small as possible.

A reference design by Texas Instruments (TI) [85] met the requirements. It can create 1ns current pulses of 60A and is especially designed for LiDAR applications. On top of this it has a flexible design so different laser diodes can be tested and easily installed. No other similar or affordable designs were found therefore this design was used as reference.

#### 4.3.1. Schematic

A simple explanation of the working principle of the laser driver of TI is that when the Gallium Nitride MOSFET (GaN FET) is turned on for a short amount of time, the drain of the FET is pulled low and shorting the laser diode for a short amount of time. This results in a short but large current pulse provided by the power capacitors. The higher the bus voltage the greater the current pulse.

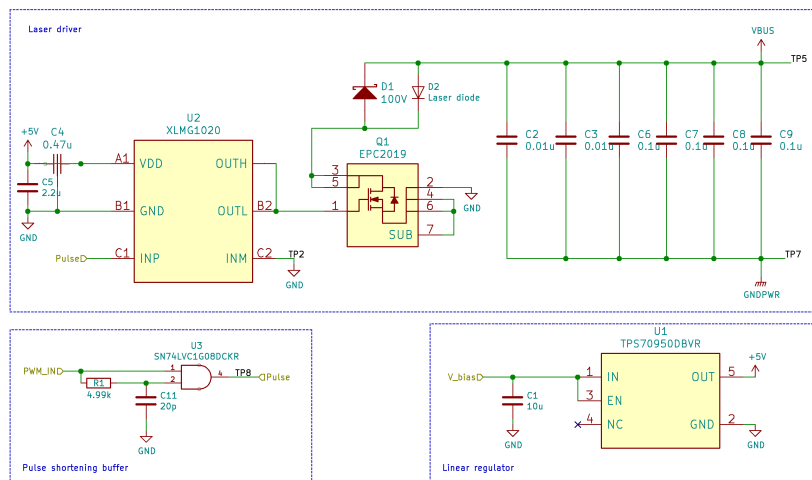


Figure 4.2: Laser driver schematic based on [85]

Some features of the laser driver are highlighted in the list below, these features also contain reasons why the decision was made to not design our own circuit.

- Capable of delivering 60A, 1-ns current pulses.  
In order to provide these currents high-frequency capacitors have been selected,  $C_2$ ,  $C_3$  and  $C_6$  up to  $C_9$ . The layout of the capacitors is critical in order to have the least amount of parasitic inductance
- Kelvin Gate.  
Since there is a high  $\frac{di}{dt}$  a lot of current is flowing in the ground, which can cause two points to be at different potentials which is equivalent to noise. A solution to preventing this ground noise is by breaking the ground noise, via lifting. The TI reference design decouples the signal ground from the power ground via the kelvin gate of the GaN FET.
- Adequate thermal management
- The circuit and PCB layout have been optimised for minimal inductance.  
Inductance is a major problem, it can significantly reduce the current peak. Therefore to minimize the parasitic inductance the layout has been made symmetrical, which is equivalent to placing the parasitic inductances in parallel, therefore decreasing the inductance. Furthermore the current loop is kept as small as possible, by using micro vias in pad and having a ground plane layer immediately adjacent to the top layer.
- Clamping diode,  $D_1$ .  
The parasitic inductance also influence the voltage waveform and can cause inductive overshoot. The energy of the inductance will be transferred to the GaN FET capacitance and cause major voltage spikes  $\frac{1}{2}V^2C = \frac{1}{2}I^2L$ . These overshoots can cause overstress in the system, therefore a clamping diode was added in parallel to the laser diode. The clamping diode was carefully selected based on board layout, capacitance and inductance.
- Pulse generator. A pulse shortening buffer is integrated in the laser driver design in order to shorten a 100 ns pulse to 1 ns. The pulse shortening buffer is more thoroughly discussed in the next section.

## 4.4. Pulse generator

In order to meet the range specifications it is crucial to create an as short as possible pulse width as already discussed in the previous section. Since the laser driver is capable of handling 1 ns pulses it was decided to aim to create a 1 ns pulse. The FPGA, selected by the receiving stage (as per requirement PER17), is capable of generating 10 ns. Therefore it is necessary to design a pulse shortening buffer.

The proposed and implemented solution by the reference design of the laser driver [85] consists of an AND gate in combination with an RC circuit, as depicted in Figure 4.3. The AND gate compares the input with an RC delayed version; when both signals are high an output signal is produced. This configuration however highly depends on the rise time of the input pulse, the pulse width and the voltage of the input pulse. This hypothesis was confirmed when tests were performed with the laser driver, results are given in the Appendix A.7. It showed the pulse at the input of the GaN FET was not very stable.

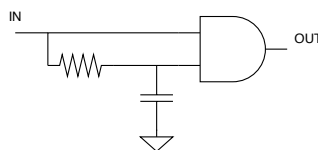


Figure 4.3: Pulse generator TI [85]

Therefore, multiple alternatives were considered for implementing a more stable system, which do not depend on the rising edge of the input nor on its amplitude. The circuits considered are all depicted in Figure 4.4 and will now be briefly discussed. Furthermore the advantages and disadvantages of each configuration will be listed.

### 4.4.1. Option A: Transmission line

A delay can be created by using the time it takes to propagate from one point to another through a transmission line. This principle can be used for short delays, since the larger the delay the more space it will take. In order to create a 1ns delay by using transmission lines the trace length will have to be around 15 cm. This length was calculated using  $t_{pd} = 85\sqrt{0.475\epsilon_r + 0.65}$  which is the propagation delay of microstrips [32]. Apart from taking up too much space, the relative permittivity of the trace also varies with temperature. This variation might result in a considerable change in propagation delay.

In order to give a short overview, the advantages and disadvantages of this solution are summed up below:

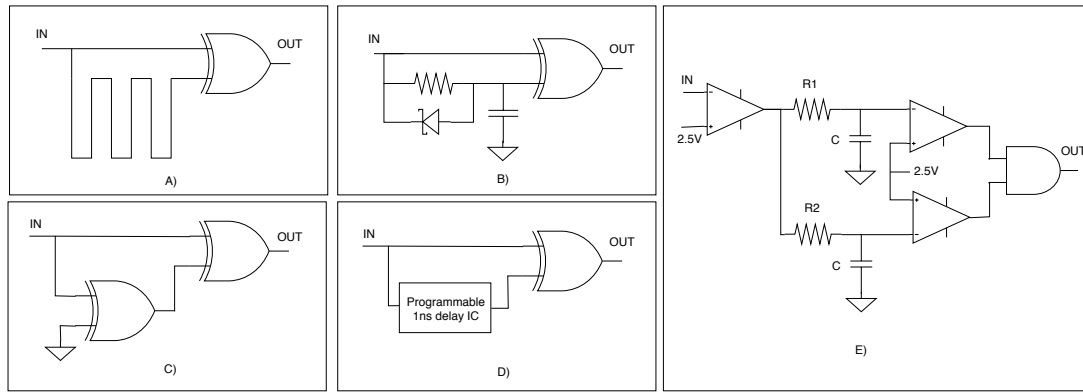


Figure 4.4: The five pulse generator circuits

- + Low cost
- + No components needed
- Large PCB footprint
- Temperature dependent pulse width

#### 4.4.2. Option B: XOR and RC configuration

In an attempt to keep the current layout of the laser driver, the following configuration was considered. The XOR gate ensures that the pulse width of the output pulse is equal to  $0.7\tau$ , with  $\tau$  being the time constant of the RC circuit. Therefore this solution will only depend on the rising edge of the input and not as with the proposed solution from TI also on the falling edge. Apart from interchanging the AND gate with a XOR gate, a diode has been added in parallel with the resistor. This diode ensures that the capacitor is discharged more rapidly. This is essential in order to reduce the probability of creating a secondary pulse.

This alternative however still depends on the rise time and amplitude of the input pulse. Furthermore, selecting a fast enough diode might be a challenge. Diodes experience a principle called recovery time and have a space charge capacitance, both these aspects limit the switching speed of diodes. Exact details about this matter can be found in the Appendix A.8.

In short the advantages and disadvantages of the configuration are listed in the list below:

- + Current PCB layout of laser driver can be used
- + Pulse width only determined by rising edge
- Secondary pulse might be generated
- Fast diode needed
- Rise time dependent
- Pulse width dependent on amplitude input
- Pulse width uncertainty due to temperature

#### 4.4.3. Option C: Double XOR configuration

The working principle of the XOR configuration is as follows, the propagation delay of the first XOR replaces the RC circuit and creates the delayed input version. The advantage of this configuration is that it requires the least amount of components; most ICs with logic gates are available containing 2 or more logic gates. A disadvantage of it is that the delay is not tunable and might vary extremely depending on the IC or the environment in which the IC is operated in.

An overview of the advantages and disadvantages of this configuration is given below in the form of a summation.

- + Simple circuitry, 1 IC
- + Low cost
- + Small footprint
- Pulse width not tunable, manufacturing dependent
- Pulse width uncertain (depends on manufacturing)
- Pulse width might vary due to pressure

#### 4.4.4. Option D: IC Delay line

Since a delay must be created the most straight forward solution would be to add a dedicated ICs for creating 1 ns delayed input versions. These IC, such as the DS1023 [45] are rather expensive and require logic signals for

programming. The delay of the IC can be programmed either via a serial communication or with 8 logic signals. Such delay lines also experience deviations from the programmed delay time. It is not known whether these deviations are systematic or random. Therefore the deviation might differ from measurement to measurement but it can also be greatly influenced by the operating environment. The XOR gate ensures that on every edge of the input signal the delay is converted to a 1 ns pulse.

As in the previous sections a short overview of the advantages and disadvantages are listed below:

- + Simple circuitry, 1 IC
- + Pulse width programmable
- + Not amplitude dependent
- + Rise time independent
- + Edge triggered
- High cost
- Large PCB footprint
- Uncertain errors
- Pulse width might vary due to pressure

#### 4.4.5. Option E: Comparator configuration

The last design considered is based upon a reference design from Analog Devices [92]. It suggests to use three comparators in combination with an AND gate. The first comparator functions as a buffer and inverter. The comparator drives a fixed and a variable RC network. The difference in charge time of the two RC networks is directly related to the pulse width of the output due to the AND gate.

Again the advantages and disadvantages are summed up below:

- + Simple adjustment of the pulse width
- + Amplitude independent
- + Rise time independent
- + Medium PCB footprint
- + Falling or Rising edge triggered
- High cost
- Large PCB footprint

### 4.5. Power converters

Power electronic converters are needed to convert the 48 V to multiple power levels, namely for the APD bias voltage, the bus voltage and bias voltage of the laser driver. The APD reverse bias will require a step-up converter, the bus voltage can either be a step-up or a step-down depending on the maximum voltage level that the laser diode can handle and the bias voltage for the laser driver requires a step-down converter. Therefore multiple power converters were researched. There are multiple DC-DC converters which can be divided into three categories: linear mode, switch mode and resonant mode. The main difference between each mode is the efficiency and the complexity of the control circuitry. Table 4.2 shows the weaknesses and strengths of each type of converter. More information about the working of each converter type will not be discussed here but can be found in the Appendix A.9. The design choice for each of the three power converters needed in the design will be discussed in the upcoming paragraphs.

Table 4.2: Comparison of Power converters

Converter	Linear mode	Switching mode	Resonant mode	Voltage multiplier
Conversion	Step-down	Step-down/Step-up	Step-down/Step-up	Step-up
Circuit complexity	Low	Medium	High	Low
Adjustable output	Simple	No	No	No
Efficiency	Low, $\frac{V_{out}}{V_{in}}$ [36]	Medium, 40-80%	High, 80-90%	Medium, 20-60%
Power dissipation	High, $(V_{in} - V_{out})I_{out}$	Low	Low	Medium
Noise	Low	Medium	Medium	Low
Size	Large, with heatsink	Small	Small	Small
Type of load	Low current, small voltage difference	-	-	Low load current, high voltage

### 4.5.1. Bus voltage

The laser driver needs a bus voltage, between 10-70V. The higher the voltage the greater the current pulse and therefore the higher the optical output power. However as already mentioned, in section 4.4, during testing of the TI laser driver it was discovered that the pulse width was not stable and this pulse width is related to the peak optical power of the laser diode. If the pulse width is smaller, the peak power can be higher. The peak power is made higher by increasing the amperage in the current pulse, which is done by increasing the bus voltage. Thus the bus voltage could also not be determined and might be higher with a smaller pulse width, how much higher is not known. On top of this, tests with the chosen laser diode also showed that the optical output power of the laser diode is not going to meet the range specifications. This will be explained further in the following chapters.

Lastly, the same test showed that the laser diode will only be capable of withstanding voltage between 10-30V. his finding will also be discussed in the coming chapters. Thus for the current design a step-down converter would suffice. However if in the future another laser diode is selected the specifications for the bus voltage converter could significantly change. Thus in order to keep the design time as limited as possible, it was decided to use an **adjustable linear voltage regulator** for the bus voltage with a voltage range of 10 to 30 V.

### 4.5.2. Bias voltage

The bias voltage needs to supply the ICs that are used in the laser driver, which all need a 5 V supply. The laser driver from TI converts an 6-15V input to steady 5V supply by means of a linear regulator.

Since the efficiency of a linear regulator declines when the difference between the input and output voltage increases it was decided to design a converter that would convert 48V to 6 V. The same reasoning was used in order to decide on the converter type. A linear regulator would be very inefficient and a resonant mode converter was too complex, therefore a **step-down switch mode converter** will be implemented for the bias voltage.

### 4.5.3. APD bias voltage

The APD bias has to drive a low load current with a high voltage of 130V. If a boost converter is used the efficiency would be very low, in the order of 20% as the Figure A.6 in the Appendix A.10 shows. Therefore it was decided to use a **voltage multiplier**, based on table 4.2.



# 5

## Implementation

The previous chapter discussed the considered designs for the deliverables. In this chapter the implementation of the chosen designs will be explained. This includes the implementation of the laser diode and the way the diode has been made pressure tolerant. Furthermore due to a redesign of the pulse generator, the laser driver also had to be adjusted. The problems that occurred during the redesign and the solutions will be discussed. The laser driver also needs two power conversions, for the bias voltage and the bus voltage. The implementations of these converters will be elaborated upon. Lastly the deliverables included a bias voltage for the APD for the receiving stage of the LiDAR.

### 5.1. Laser Diode

Given the set requirements for the laser diodes in section 4.1.3, an adequate laser diode has to be searched in the market. After some research, the chosen laser diode was the PLT5 520B by Osram. The following specifications of this laser diode are as follows [4]

1. Average optical output power is 50 mW and the peak optical output power is around 80 mW
2. Beam divergence of the laser diode is typically 6.3° perpendicular and 22.5° parallel to the pn junction of the laser diode
3. The wavelength range of the laser diode is between 515 and 530 nm.

Since this laser diode comes in a specific packaging, the laser diode was modified and certain elements were added alongside to meet the set requirements as per chapter 3. These modifications and additions are elaborated upon in forthcoming sections.

#### 5.1.1. Pressure tolerance

As per requirement ENV1-a, the system should withstand a pressure higher than 100 bar. Since the chosen green laser diode, PLT5 520B, has a gas pocket in its package, this is hazardous for the laser diode as this gas pocket will implode under high pressure. The solution to this issue was to decan the laser diode, this will remove the gas pocket [65]. Figure 5.1 depicts a canned and a decanned laser diode. The decanned laser diode has to be submerged in a liquid, as per requirement PER16 on top of this long exposure to air will lead to facet oxidation and eventually to a decreased optical output power [67].

#### 5.1.2. Focusing lens and heatsink

Since the laser diode has a beam divergence characteristic, the laser beam should therefore be collimated into one consistent laser beam to ensure there are no optical power losses. Focusing lens is needed in order to achieve this [65] and the one used for the laser diode is the C330TMD-A focusing lens from Thorlabs.

When analysing the pulse power of the laser diode, it can be deduced that high pulse power may cause thermal problems for the laser diode. This can occur as the small package of the laser diode does not ensure adequate thermal control. Therefore, the laser diode was encased in a heatsink to achieve the necessary thermal control. Figure 5.2 depicts the encased laser diode.



Figure 5.1: Figure depicting a normal laser diode and a de-canned laser diode

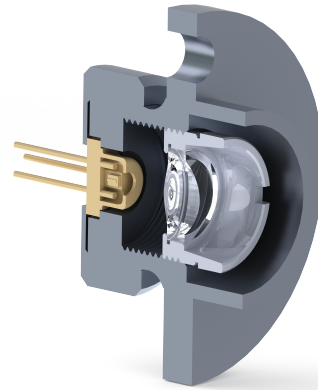


Figure 5.2: Laser diode which is encased by the heatsink. The focusing lens resides within the encasing.

## 5.2. Laser driver

The pulse shortening buffer used in the laser driver from TI was not stable, therefore as given in the previous chapter other pulse shortening buffers were designed. Since the pulses are 1 ns long, the current loop must be kept as small as possible to avoid parasitic inductances. Therefore the laser driver had to be refabricated. The schematic and layout of the new design closely resembles the schematic in Figure 4.2, and layout as given by TI [85]. The main differences are the pulse generator and the replacement of the micro vias. The exact changes made are discussed below.

### 5.2.1. Micro vias

Micro vias are vias that have a smaller hole diameter and are not through-hole. The main advantage of this is that the vias can be placed in pad and there is no stub, which could form an impedance when operating at very high frequencies. The main reason for using micro-vias is to keep the inductance of the VDD source and return path as well as the gate return loop as small as possible. Micro vias are however very expensive, it will cost about 1000 € to refabricate the laser driver. Therefore it was decided to research the effect of placing through-hole vias off pad. The stub created by the through-hole via is smaller than a tenth of the wavelength,  $\frac{\lambda}{10}$ , thus the stub should not introduce extra inductance. Placing the vias off pad makes the current path larger, which could lead to more inductance. The current path is however already extremely reduced when the onboard resistive load is removed. This allows the power capacitors to be placed closer to the laser diode. Therefore in order to reduce the cost it was decided to try to replace the microvias with through hole vias off pad.

Another aspect that must be considered is the fact that placing the vias off pad could also result in ground bouncing. This could result in the GaN FET being turned on and off continuously.

### 5.2.2. Pulse generator

Based on the advantages and disadvantages mentioned in the previous chapter, the pulse shortening buffer of option E, section 4.4.5, was selected. Some small improvements were made, as given in the final schematic in Figure 5.3 and listed below.

- A variable resistor  $RV$ , ensures that the pulse width can be tuned, in theory between from 0 to 3 ns, and allows to switch between rising edge or falling edge triggering. This time difference follows from the difference in time constant of the RC circuits:  $T_{pulse} = 0.7 * C * \Delta R$
- The gate driver included in the laser driver, LMG1020, has an integrated AND gate with an inverted input. This AND gate is used to create the output pulse.

The schematic was simulated, without the actual LMG1020, which showed that the circuit should work. The simulations are given in the Appendix A.11.

## 5.3. Bus voltage

As explained in the previous chapter, the bus voltage will be generated by using a linear regulator and will have a voltage range of 10 to 30 V. After a parametric search a simple low cost linear voltage regulator was chosen, the

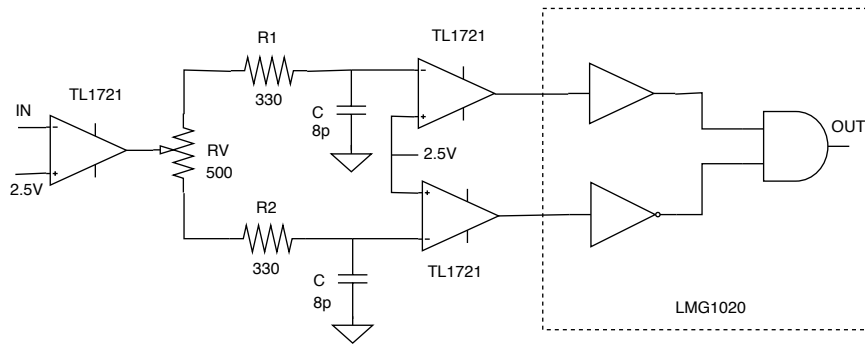


Figure 5.3: Pulse generator

TL783 from Texas Instruments. The schematic of the linear regulator is given in Figure 5.5. The key point of this voltage regulator are listed as follow :

1. Simple design and implementation of the circuitry
2. Cost is 1.78 €

One of the main concerns for the design of the linear voltage is the power dissipated in the voltage regulator. As explained in section A.9.1, the efficiency can be calculated. Knowing the minimum output voltage is 10 V and the input voltage is 48 V, the efficiency in worst case scenario is  $\eta = \frac{10}{48} \cdot 100 \approx 20\%$ . As expected the efficiency will be very low. The power dissipated in the linear regulator will in the worst case be equal to  $P_{\text{loss}} = 0.8 \cdot (48 - 10) \cdot 0.1 \approx 3.8\text{W}$ . Therefore a heatsink might not be needed, but has been integrated in the design just in case. The PCB design of the bus voltage is given in Appendix A.15 and the explanation for the component values is given in Appendix A.14.

## 5.4. Bias voltage

For the bias voltage for the laser driver, the requirement of the laser driver is to supply a voltage between 5 to 15 V for the bias voltage [85]. As already stated in section 4.5.2, a buck converter will be implemented to supply the bias voltage. After weighing up the options of buck converters, the chosen buck converter IC was the LM5166 from Texas Instruments [84]. The key points of this buck converter are as follow :

1. Efficiency of 83 %
2. Cost is 2.95 €
3. Low component count

Knowing the set output voltage, the buck converter was designed and the schematic is given in figure 5.4. The explanation for each component values is given in Appendix A.13 and the design of the PCB is given in Appendix A.15.

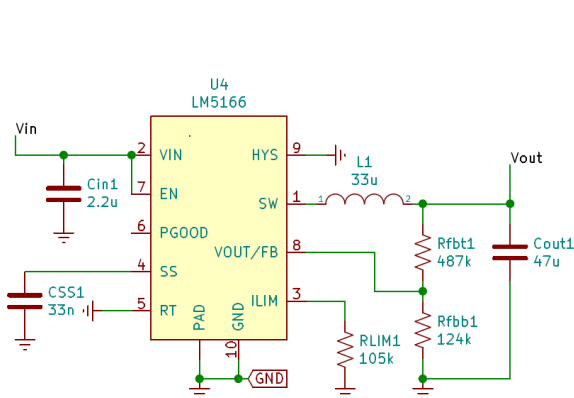


Figure 5.4: Schematic of the circuit which will supply the bias voltage

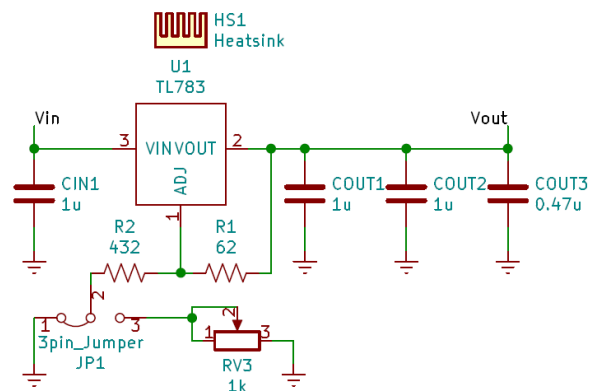


Figure 5.5: Schematic of the circuit which will supply the bus voltage

## 5.5. APD bias voltage

To meet the set requirements PER15, 130V with a load current of 5 mA, the decision was made to design a voltage multiplier. Since the supply voltage is 48V, a voltage needs to be tripled. The schematic and PCB layout of the voltage tripler will now be discussed.

### 5.5.1. Schematic

The Schematic, as given in Figure 5.6, can be separated in three parts. The actual voltage tripler, the pulse generator and a linear regulator. The implementation of each of the three parts will now be elaborated.

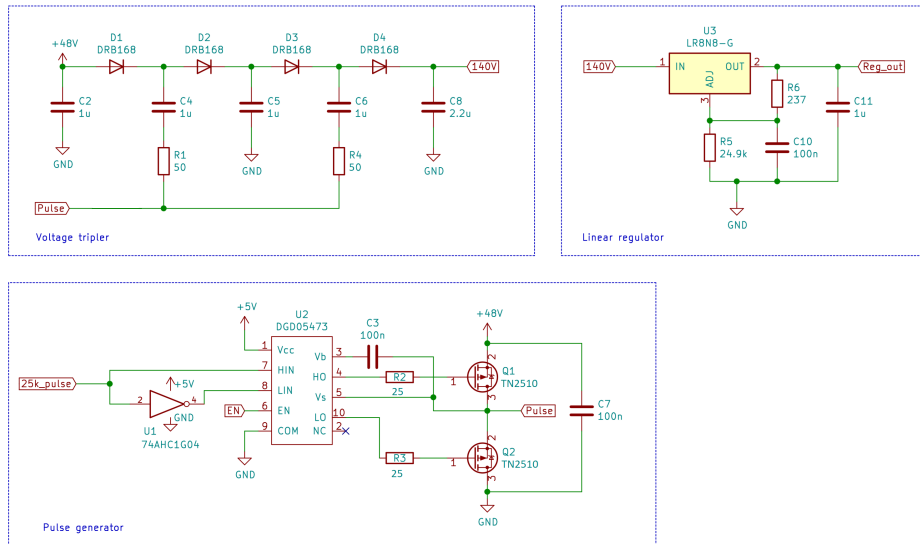


Figure 5.6: Schematic of the APD bias

### Voltage tripler

The voltage tripler is based on a bootstrap configuration. To explain the working principle of the voltage tripler will just look at a small the section of the schematic, consisting of  $C_4$ ,  $C_5$ ,  $D_1$  and  $D_2$ . During the low cycle of the input waveform, *Pulse*, capacitors  $C_4$  and  $C_5$  are charged to  $48 - V_{drop}$  V. During the positive cycle, the diode  $D_1$  blocks the discharge of capacitor  $C_4$ , while diode  $D_2$  allows the charging up of capacitor  $C_5$ . The voltage across capacitor  $C_5$  however is already equal to  $48 - V_{drop}$  V, therefore  $C_5$  charges to twice  $48 - V_{drop}$ , which results in a voltage doubling. The same principle ensures that the capacitor  $C_8$  is charged up to 144 V.

The first task was to find a suitable diode capable of withstanding the large reverse voltages of 130 V and with a suitable SPICE model. After searching what kind of diodes are available that still suffice the minimum requirements, the RB168 [21] schottky diode was selected. The most important device parameters are listed below ordered by importance.

- Repetitive reverse bias voltage: 150 V
- Forward voltage: 0.89 V
- Forward current: 1 A
- Footprint: sot-323HE
- Cost: 0.33 €

Next the capacitors have to be selected. In most voltage multiplier designs it is best to use electrolyte capacitors, since these have a high and stable capacitance with high bias voltages and are inexpensive. However the design must be pressure tolerant. Electrolytic capacitors can not be used, since these contain an air pocket. Thus it can not with stand high pressure. Therefore a suitable ceramic capacitors had to be found. The capacitance is however very dependent on the applied bias voltage. Therefore a parametric search was conducted, focusing on two aspects: a high capacitance at the applied bias voltage and not too expensive.

With the capacitor values selected and the actual capacitance values at the applied bias voltage known, simulations were run to check whether the output voltage would experience a large ripple. The result of the simulation is given in Figure 5.7.

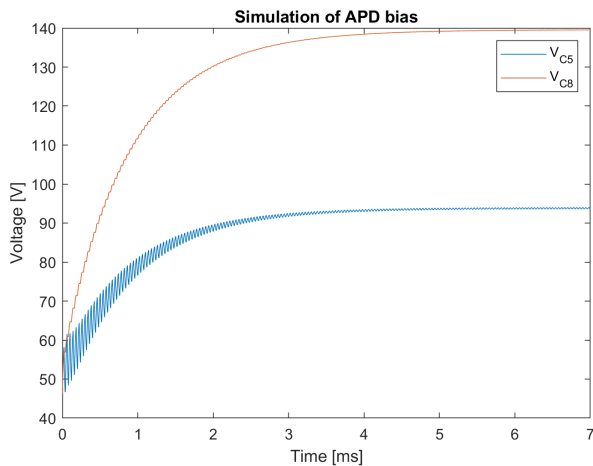


Figure 5.7: APD bias voltage simulation

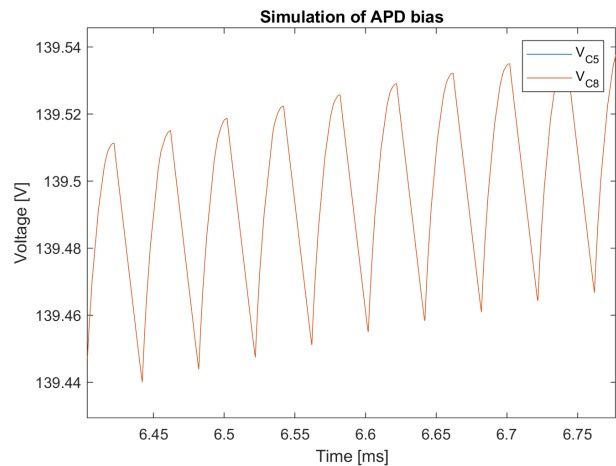


Figure 5.8: APD bias voltage simulation close up

Figure 5.8 shows an output ripple of 83 mV, which is relatively low and can even be improved if a linear voltage regulator is placed in series. Therefore it was concluded that this circuit would suffice and the design was continued.

In order to limit the peak currents during switching, the resistor  $R_1$  and  $R_4$  were needed. Since the current through a capacitor is directly related to the change in voltage. Therefore without the resistors this current would be very large, which is bad for EMI.

### Pulse generator

In order for the voltage tripler to work a PWM pulse with 48 V<sub>pp</sub> square wave is needed. This charges the capacitors  $C_5$  to  $2 * V_{in} - 2V_{drop}$  and  $C_7$  to  $3 * V_{in} - 4V_{drop}$ ,  $V_{drop}$  is the voltage drop over the diode. There is some leakage and if it is not periodically recharged the output ripple would increase.

The 48V<sub>pp</sub> square wave is realised by using a metal-oxide-semiconductor field-effect transistor (MOSFET) half bridge configuration. The TN2510, [72], n-channel metal-oxide-semiconductor field-effect transistors (nMOSFETs) have been selected in order to create the half bridge based on the following parameters (in order of importance):

- Pulsed drain current: 5.0 A
- Threshold voltage: 2.0 V
- Maximum power dissipation: 1.6 W
- Drain-to-source on resistance: 2.0  $\Omega$
- Cost: 0.89€ per piece
- Package: P-SOD-89-3

In order to drive the half-bridge a MOSFET gate driver is used. The gate driver switches the MOSFETs on or off based on the logic input signals. After a parametric search the gate driver selected was the DGD05473 [29], which is inexpensive, 0.699€ per piece, can handle 3.3V logic input signals and can be supplied with 5 V. Lastly, an inverter was needed at the input of the gate driver, to ensure that the MOSFETs  $Q_1$  and  $Q_2$  receive inverted gate voltages and to be able to control the gate driver with only one PWM signal. The inverter selected is just a basic inverter, capable of switching at at least 25kHz with an easy package to solder.

### Linear regulator

Due to the discharging and charging of the capacitor  $C_5$  and  $C_8$  the output voltage will have a ripple, this is one of the disadvantages of this circuit. In case the output ripple of the voltage tripler is too large for the APD, the option was created to be able to add a linear voltage regulator in series with the output of the voltage tripler. The linear voltage regulator selected, LR8N8 [91], has a ripple rejection ratio of 40-60 dB, therefore the ripple is at least reduced with

a factor of 100. The schematic of the linear regulator is very straight forward, the resistor values of  $R_5$  and  $R_6$  were chosen in such a way that the minimum output current of 0.5mA is always met and that the output voltage is less than  $144 - V_{drop} - 4 * V_{drop}$ .

## Testing and Validation

The working of the system as described in the previous chapter has been tested in order to validate the overall working of the system. Firstly all the subsystems were tested separately and here after the full system was tested. Once the system worked with a low bus voltage, this voltage was increased to find the maximally reachable optical output power of the laser diode.

### 6.1. Laser diode

The goal for the laser diode, was to find a COTS green laser diode with high optical output power and design it to be pressure tolerant. In order to check the optical output power of the laser diode the full system is needed. Therefore this measurement is discussed in the last section of this chapter. It has been discussed that the laser diode was decanned in order to remove the air pocket. The decanned laser diode will then be exposed to either of four liquids. These liquids could chemically alter the laser diode or could influence the reflectivity of the laser surface. Therefore two tests were performed. A third test with a decanned laser diode was made to check for the pressure tolerance.

#### 6.1.1. Pressure tolerance integration

In the first test four laser diodes were submerged for a few minutes in one of the three liquids. As table 6.1 shows, that two of the liquids chemically altered the laser diode.

The second test, when the laser was turned on while in the liquid, showed that the functionality of the laser diode was not altered due to the reflectivity of the liquid. The results are also given in table 6.1.

Table 6.1: Measurement result of laser diode

Liquid	Zero measurement	Passive test results	Active test results
IPA	0.19 mW	0.09mW	23.0 uW
Mineral oil	0.17 mW	0.00 mW	18.1 uW
FC-770	0.22 mW	0.22 mW	0.17 mW
Diode with epoxy	0.28 mW	0.29 mW	0.30 mW

#### 6.1.2. Pressure test of the laser diode

In the second test, a laser diode was decanned and encased in the heat sink encasing alongside the focusing lens. Next the laser system was placed in a pressure chamber and the pressure in the chamber was gradually increased till 100 bar. Lastly, the performance of the laser was analysed as the pressure inside the chamber was increasing. Figures 6.1 and 6.2 depict the laser beam at 0 bar and at 100 bar.

The figure above does depict a difference between the shape and the direction of the laser beam at different pressure levels, yet this alteration is very small and will not hamper the overall performance of the LiDAR system. Furthermore, the altered laser beam was not permanent as the laser beam shape and direction reverted back to its original characteristics when the pressure level was set back to 0 bar. Reasons as to why there is a slight change in the laser beam are presumed to be as follows:

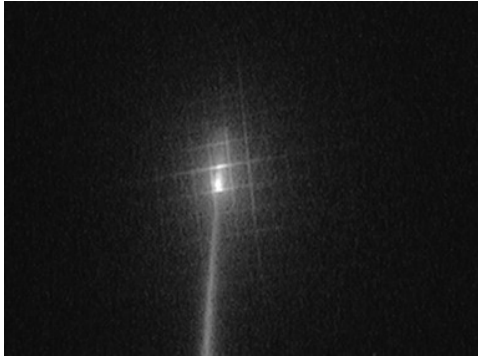


Figure 6.1: Laser beam at a pressure level of 0 bar

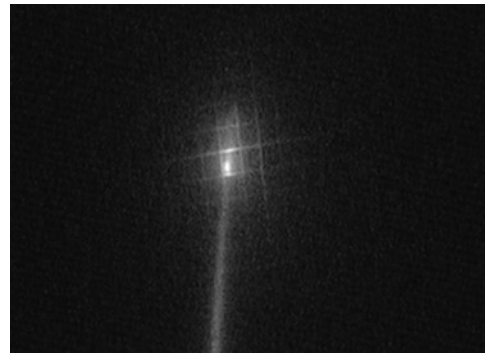


Figure 6.2: Laser beam at a pressure level of 100 bar

- Characteristics of the laser diode gradually changed or the laser diode was slowly changed from its position while the pressure levels were increasing
- Likewise for the focusing lens

## 6.2. Pulse generator

The goal for the redesign of the pulse generator was to create a stable pulse with a width of 3 ns or less, the pulse width had to be independent of the rise time and amplitude of the incoming control signal from the FPGA. Since the FPGA is capable of producing a 3.3V<sub>pp</sub> 25 kHz square wave with 0.25% duty cycle, the circuit was tested with such a wave. The test results as shown in Figure 6.3. It shows that the pulse generator is capable of creating a 3 ns or larger pulse width. It is not possible to create smaller pulse widths, the output voltage of the LMG1020 decreases significantly if the pulse width is decreased. This shows that the LMG1020 is not able to drive the GaN FET with smaller pulses. Therefore it is not possible to meet requirement TX-PER3a with the current laser driver. Solutions to this problem are discussed in Future work 7.

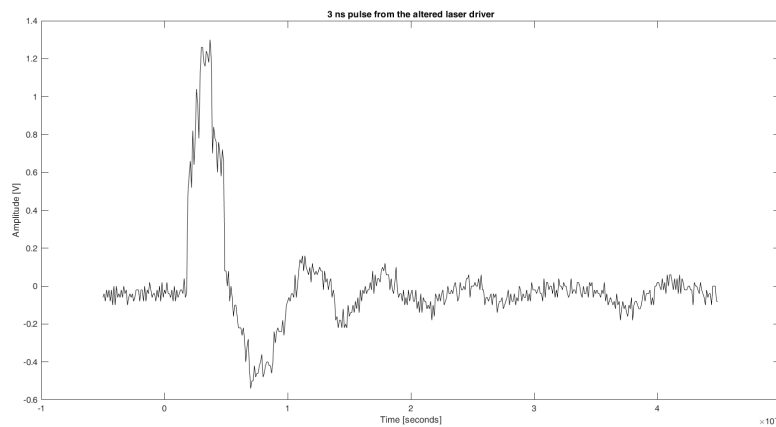


Figure 6.3: Pulse generator output signal close up

## 6.3. Bus and bias voltage

The test and validation for both PCB's for the bias and bus voltage were conducted under same set input values. The sole input being an input voltage of 48 V and the output voltage of both implementations were read out at the test points of the PCB. The results are given as follow.

1. Bus voltage  
The measured voltage range at the output was between 10.10 and 30.75 V.
2. Bias voltage  
The measured voltage at the output of PCB was 6.06 V.

From these measured values, it can be deduced that both the bus voltage and bias voltage PCB functions properly.

## 6.4. Laser driver

The laser driver was redesigned. To ensure whether the changes resulted in an increase of parasitic inductances, which would negatively influence the performance of the laser driver and laser diode, the inductive overshoot at the drain voltage of the GaN FET was measured. A second test was performed to verify whether the optical output pulse power of the laser diode met the requirement TX-PER2.

### 6.4.1. Inductive overshoot

The first measurement performed on the laser driver, was to check whether the redesign of the laser driver resulted in an increase of inductance. This could lead to inductive overshoot that could result in a too high of a reverse voltage over the laser diode. The measurement results of the laser driver are shown in Figure 6.4. From this figure it is possible to conclude that the laser driver does not experience overshoot at low bus voltages. Another conclusion can also be drawn, the replacement of the micro vias did not result in more ground bouncing.

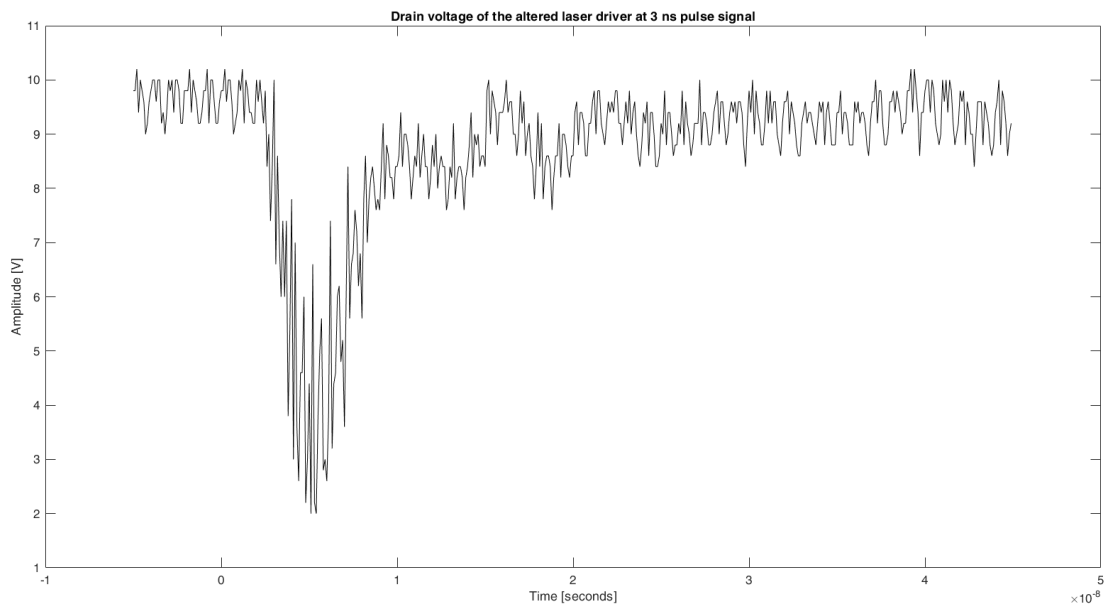


Figure 6.4: Laser driver, drain voltage

### 6.4.2. Optical output power

The main goal of the thesis was to create pulses of light with a high optical output power in order to be able to detect objects at a range of at least 10m. This range is highly dependent on the receiving stage of the LiDAR, but for now at least the maximum optical output power of the laser diode in combination with the laser driver and its converters can be measured. In order to damage the least amount of laser diodes, the repetition frequency and bus voltage were slowly scaled up until the requirements were met or the laser diode failed.

This measurement was done early on in the design process to get a grip on the pulse power that would be achieved with the laser diode that had been selected. At this stage the laser driver from TI was used, since it still had to be redesigned. The upscaling of the frequency gave the graphic result as presented in Figure 6.5. This figure shows that if the frequency is increased, the peak pulse power decreases. The other conclusion that could be drawn, was that the optical output of the laser diode saturates between a bus voltage of 15-20V. And lastly the figure shows that two different laser diodes, produce different optical output powers.

A comparable measurement has been made with the redesigned laser driver. Here the repetition frequency was kept at 25 kHz, since 25 kHz meets the requirements PER14-A and increasing the frequency greatly decreases the optical output power in a pulse. The pulse power measured from the laser driver is compared with the pulse power of the TI laser driver in Figure 6.6. These results show that a smaller pulse width does have a significant influence on the optical power in one pulse. But more importantly, the redesigned laser driver performs better than the laser driver from TI.

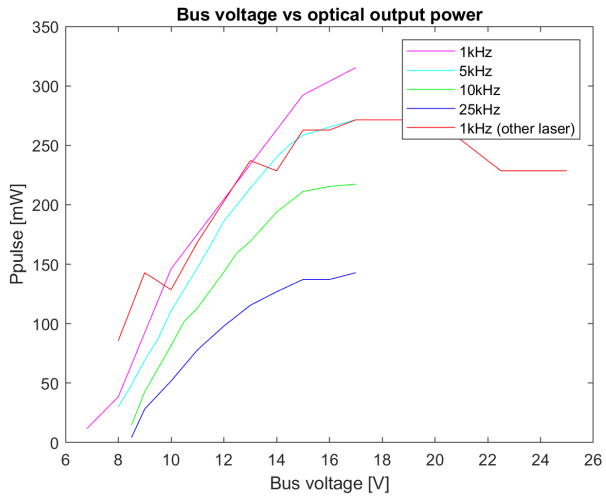


Figure 6.5: Frequency versus Bus voltage

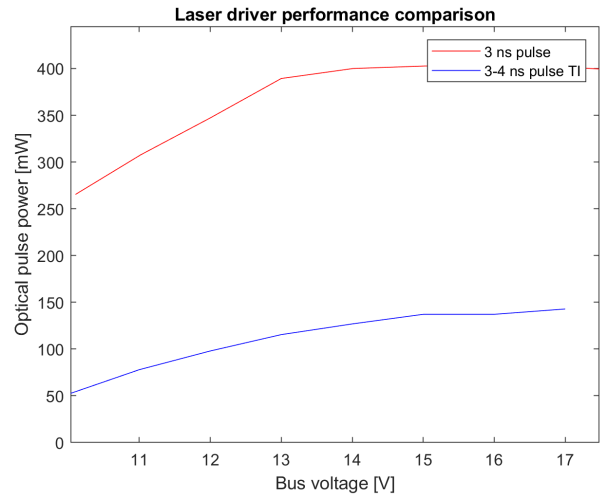


Figure 6.6: Laser driver comparison

## 6.5. APD bias voltage

Lastly, the APD bias voltage. Due to initial layout errors and difficulties in placing the gate driver, the half-bridge configuration was not able to produce the  $48V_{pp}$  square wave needed to power the voltage multiplier. However when the voltage multiplier receives a square wave it does triple the given input voltage.

# 7

## Conclusion

The main goal was to create a deepsea LiDAR system suitable for SLAM. Therefore multiple architectures were researched and a subsystem division was made. The main focus of this thesis is centered around the transmission stage of the LiDAR system. The designed transmission stage consists of a laser diode, driver and multiple power converters.

A laser diode has been selected based on high optical output power and has been made pressure tolerant. It is driven by a laser driver, based on the reference design of Texas Instruments. The design had to be altered, since the pulse width varied with the input amplitude. It was successfully altered to create stable and smaller current pulses of 3 ns. Further testing of this showed that the altered version of the laser driver (with the new pulse generator) performed better than the laser driver of Texas Instruments, as explained in section 6.2. A follow up test was done in order to determine the optimal bus voltage for the laser diode in order to achieve the highest optical output power of the laser diode, which was explained in section 6.4.2. The results showed that there is a dropoff of laser performance when the bus voltage is higher than 15 V.

The laser driver needs multiple voltages, which all need to be converted from 48V. For this a buck converter and linear regulator have been designed and successfully implemented. Lastly, as part of this thesis a high voltage bias needed to power the photodiode, as selected by the receiving stage, had to be designed. This converter needed to supply 130 V with a 5 mA load. This was implemented using a voltage multiplier. The circuit was designed, simulated and fabricated, yet the component selection did not take into account the package types. Therefore the PCB layout could not be assembled easily. Therefore the half-bridge configuration was not capable of producing a  $48V_{pp}$  square wave and this could not be correct within the timeframe of the project.

### 7.1. Future work

In this section, future optimizations for the transmit stage of the LiDAR is discussed. Furthermore, optimizations for the overall LiDAR system is discussed based on the results that were acquired during the testing of the LiDAR.

#### 7.1.1. Transmit stage

The main challenge left for future work of this specific thesis is the replacement of the current laser diode with a higher power rated laser diode, the current laser diode clearly lacks the ability to produce enough power to meet the requirement TX-PER3a. Since there are no green laser diodes in the market with a higher power. The option of using an infrared laser in combination with a frequency doubling crystal needs to be explored further. The integration of a frequency doubling requires more research focused on determining the efficiency that could be reached with such a crystal. The replacement of the laser diode will also influence the design of the bus voltage. For a commercially viable product the design of the bus voltage would already have to be replaced with a more efficient buck converter.

Still another improvement might be found in further reducing the pulse width. The current limitation is that the LMG1020 is not capable of pulling the gate voltage high enough for the GaN FET to turn fully on when smaller pulse widths are used. Either replacement of the LMG1020 with another gate driver will or the replacement of the GaN FET might resolve this issue. Another option would be to use an entirely different laser driver configuration, further research must be conducted to check whether this is possible.

Lastly, the voltage multiplier for the APD bias voltage currently does not work. A quick fix would be to replace the current gate driver with a working sample. This package is however very tedious to place and thus it is recommended

to redesign the PCB layout and choose a different gate driver package that is more easily replaced. This would make it more prototype friendly. Furthermore the current design uses a bootstrap configuration, which needs capacitors capable of with standing high bias voltages. It might be better to use a cockcroft-walton multiplier, since here the capacitors are placed in series and only need to operate at a bias voltage of 48V, which would reduce the capacitor size and also reduce the cost. Further research must be conducted to validate whether the cockcroft-walton is also capable of reaching a higher efficiency.

### **7.1.2. LiDAR**

Given the multitude of challenges that each subsystem faced during the timespan of the project, it was no longer feasible to test the whole LiDAR system with each subsystem integrated in the system. Therefore, an overview of all of the future optimizations for the LiDAR could not be made. Yet, a test of the whole LiDAR system should be conducted in the near future.

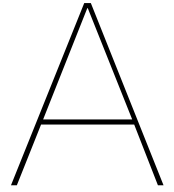
# Bibliography

- [1] 2GRobotics. *ULS-500 PRO Dynamic Underwater Laser Scanner*. URL: <https://www.2grobotics.com/products/underwater-laser-scanner-uls-500/>.
- [2] J.Peng et al. *Laser in medicine*. 2008, pp. 3–7.
- [3] A. Almslmany et al. “Time varying gain amplifier linearity enhancement for wide dynamic range in radar receiver”. In: *Proceedings of 2015 IEEE MTT-S International Conference on Numerical Electromagnetic and Multiphysics Modeling and Optimization, NEMO 2015*. IEEE, Aug. 2016, pp. 1–4. ISBN: 9781479968114. DOI: 10.1109/NEMO.2015.7415022. URL: <http://ieeexplore.ieee.org/document/7415022/>.
- [4] Biomedical Applications and Safety Advice. “Green Laser Diode in TO56 Package”. In: (2007), pp. 1–7.
- [5] Ery Arias-Castro and Yonina C. Eldar. “Noise folding in compressed sensing”. In: *IEEE Signal Processing Letters* 18.8 (2011), pp. 478–481. ISSN: 10709908. DOI: 10.1109/LSP.2011.2159837.
- [6] Shlomi Arnon. “Underwater optical wireless communication network”. In: *Optical Engineering* 49.1 (2010), p. 015001. ISSN: 0091-3286. DOI: 10.1117/1.3280288. URL: <http://opticalengineering.spiedigitallibrary.org/article.aspx?doi=10.1117/1.3280288>.
- [7] M. Riordan B. Nakamura. “The Green Lasers Semiconductors can generate laser light in all colors could soon make brilliant full-spectrum displays a reality”. In: (2009).
- [8] W.L. Barber and E.R. Brown. “A true logarithmic amplifier for radar IF applications”. In: *IEEE Journal of Solid-State Circuits* 15.3 (June 1980), pp. 291–295. ISSN: 0018-9200. DOI: 10.1109/JSSC.1980.1051386. URL: <http://ieeexplore.ieee.org/document/1051386/>.
- [9] *Blackmore LiDAR*. URL: <https://blackmoreinc.com/afdl> (visited on 06/16/2019).
- [10] Boyd. *Nonlinear Optics, Third Edition*. 2008. ISBN: 0123694701.
- [11] V. Brandou et al. “3D Reconstruction of Natural Underwater Scenes Using the Stereovision System IRIS”. In: *OCEANS 2007 - Europe*. IEEE, June 2007, pp. 1–6. ISBN: 978-1-4244-0634-0. DOI: 10.1109/oceans.2007.4302315. URL: <http://ieeexplore.ieee.org/document/4302315/>.
- [12] J.D.A. van den Broek. “Design and implementation of an Analog-to-Time-to-Digital converter”. PhD thesis. UT Twente, 2012. URL: <http://essay.utwente.nl/69501/1/MSc.%20report%20Broek%20van%20den,%20J.D.A.pdf>.
- [13] J. H.R. Burns and D. Delparte. “Comparison of commercial structure-from-motion photogrammetry software used for underwater three-dimensional modeling of coral reef environments”. In: *International Archives of the Photogrammetry, Remote Sensing and Spatial Information Sciences - ISPRS Archives*. Vol. 42. 2W3. Feb. 2017, pp. 127–131. DOI: 10.5194/isprs-archives-XLII-2-W3-127-2017. URL: <https://www.int-arch-photogramm-remote-sens-spatial-inf-sci.net/XLII-2-W3/127/2017/>.
- [14] F. M. Caimi and F. R. Dalgleish. “Performance considerations for continuous-wave and pulsed laser line scan (LLS) imaging systems”. In: *Journal of the European Optical Society* 5 (Apr. 2010), 10020s. ISSN: 19902573. DOI: 10.2971/jeos.2010.10020s. URL: [https://www.jeos.org/index.php/jeos%7B%5C\\_%7Drp/article/view/10020s](https://www.jeos.org/index.php/jeos%7B%5C_%7Drp/article/view/10020s).
- [15] Jonathan L. Carrivick and Mark W. Smith. “Fluvial and aquatic applications of Structure from Motion photogrammetry and unmanned aerial vehicle/drone technology”. In: *Wiley Interdisciplinary Reviews: Water* 6.1 (Jan. 2019), e1328. ISSN: 2049-1948. DOI: 10.1002/wat2.1328. URL: <https://onlinelibrary.wiley.com/doi/abs/10.1002/wat2.1328>.
- [16] *Coda Octopus, sound underwater intelligence*. URL: <https://www.codaoctopus.com/>.
- [17] Ryan Cole. “Construction and Optimization of a Tapered Amplifier System for Applications in Ultra-Cold Plasma Research”. In: (2015).
- [18] Albert Dato and Velimir Radmilovic. “(12) Patent Application Publication (10) Pub. No.: US 2010/0301212 A1”. In: 1.19 (2010).
- [19] DeepSea Power & Light. *Subsea Cameras*. URL: <http://www.deepsea.com/products/cameras/> (visited on 07/12/2019).
- [20] 3D at Depth. *SL3 Subsea LiDAR Laser*. URL: <https://www.3datdepth.com/product/subsea-lidar-sl3>.

- [21] Schottky Barrier Diode and Inner Circuit. "RB168MM150". In: (2017).
- [22] *EDFA explanation*. URL: <https://www.youtube.com/watch?v=4RBcELrTfIM>.
- [23] Edgetech. *EdgeTech Sonar*. URL: <https://www.edgetech.com/products/side-scan-sonar/>.
- [24] Andrew Filisetti et al. "Developments and applications of underwater LiDAR systems in support of marine science". In: *OCEANS 2018 MTS/IEEE Charleston, OCEAN 2018 January* (2019), pp. 1–10. DOI: 10.1109/OCEANS.2018.8604547.
- [25] Macera Giuseppe and Analog Devices. "U niversit à degli S tudi di N apoli F ederico II Facoltà di Ingegneria Corso : Integrated Photonic". In: May (2015). DOI: 10.13140/RG.2.1.1861.7761.
- [26] Miles Hansard et al. *Time of Flight Cameras : Principles , Methods , and Applications*. 2012. DOI: 10.1007/978-1-4471-4658-2. URL: <https://hal.inria.fr/hal-00725654/PDF/TOF.pdf>.
- [27] Duo-Min He and Gerald G.L. Seet. "Divergent-beam Lidar imaging in turbid water". In: *Optics and Lasers in Engineering* 41.1 (Jan. 2004), pp. 217–231. ISSN: 0143-8166. DOI: 10.1016/S0143-8166(02)00138-0. URL: <https://www.sciencedirect.com.tudelft.idm.oclc.org/science/article/pii/S0143816602001380>.
- [28] Franco Hidalgo and Thomas Braunl. "Review of underwater SLAM techniques". In: *ICARA 2015 - Proceedings of the 2015 6th International Conference on Automation, Robotics and Applications*. IEEE, Feb. 2015, pp. 306–311. ISBN: 9781479964666. DOI: 10.1109/ICARA.2015.7081165. URL: <http://ieeexplore.ieee.org/document/7081165/>.
- [29] High Frequency High-side, Low-side Gate Driver, and I N W-dfn- Type. "DGD05473 Pin Assignments". In: 10.June (2018), pp. 1–11.
- [30] W. Krupke J. Coleman. *Laser program annual report: Volume 1*. Lawrence Livermore National Laboratory, 1980.
- [31] Juliza Jamaludin et al. "Analysis on the performance of led and laser diode with charge coupled device (CCD) linear sensor measuring diameter of object". In: *Jurnal Teknologi* 77.17 (2015), pp. 19–25. ISSN: 01279696. DOI: 10.11113/jt.v77.6418.
- [32] H.W. Johnson and J. Graham. *High-Speed digital design: A handbook of black magic*. 1999.
- [33] Achuta Kadambi and Petros T. Boufounos. "Coded aperture compressive 3-D LIDAR". In: *ICASSP, IEEE International Conference on Acoustics, Speech and Signal Processing - Proceedings 2015-Augus* (2015), pp. 1166–1170. ISSN: 15206149. DOI: 10.1109/ICASSP.2015.7178153.
- [34] LeddarTech. *Leddar Optical Time-Of-Flight Sensing Technology*. 2016.
- [35] B. Timothy Lee. "How 10 leading companies are trying to make powerful, low-cost lida". In: *Ars Technica* (2019). URL: <https://arstechnica.com/cars/2019/02/the-ars-technica-guide-to-the-lidar-industry/>.
- [36] B.S. Lee. "Understanding the Terms and Definitions of LDO Voltage Regulators". In: (1999).
- [37] Larry Li. *Time-of-Flight Camera—An Introduction*. 2014.
- [38] Jerry Liao. *Bar code reader with polygon mirror having curved reflection surfaces*. Sept. 2005. URL: <https://patents.google.com/patent/US20070069025>.
- [39] Daniel J. Lum, Samuel H. Knarr, and John C. Howell. "Frequency-modulated continuous-wave LiDAR compressive depth-mapping". In: *Optics Express* 26.12 (June 2018), p. 15420. ISSN: 1094-4087. DOI: 10.1364/OE.26.015420. URL: <https://www.osapublishing.org/abstract.cfm?URI=oe-26-12-15420>.
- [40] Neil Manning. *Teledyne CDL*. 2014.
- [41] S. Mappus. "Synchronous Rectification for Forward Converters". In: (2010).
- [42] Marco Reps. *All about the Xiaomi Lidar Scanner and the Sunfounder RasPad*. URL: <https://www.youtube.com/watch?v=4sQCz75BfrM> (visited on 06/18/2019).
- [43] Gerald F. Marshall and Glenn E. Stutz. *Polygonal Scanners: Components, Performance, and Design*. 2011, p. 788. ISBN: 1439808791. URL: <http://books.google.com/books?id=MLWUatLv0s0C%7B%5C%7Dpgis=1>.
- [44] Miquel Massot-Campos and Gabriel Oliver-Codina. "Optical Sensors and Methods for Underwater 3D Reconstruction." In: *Sensors (Basel, Switzerland)* 15.12 (Dec. 2015), pp. 31525–57. ISSN: 1424-8220. DOI: 10.3390/s151229864. URL: <http://www.ncbi.nlm.nih.gov/pubmed/26694389%20http://www.pubmedcentral.nih.gov/articlerender.fcgi?artid=PMC4721784>.
- [45] Maxim. "8-Bit Programmable Timing Element DS1124". In: (2009), pp. 1–16.
- [46] Paul F. McManamon et al. "Comparison of flash lidar detector options". In: *Optical Engineering* 56.3 (2017), p. 031223. ISSN: 0091-3286. DOI: 10.1117/1.oe.56.3.031223.

- [47] L. E. Mertens and F. S. Replogle. "Use of point spread and beam spread functions for analysis of imaging systems in water". In: *Journal of the Optical Society of America* 67.8 (Aug. 1977), p. 1105. ISSN: 0030-3941. DOI: 10.1364/josa.67.001105. URL: <https://www.osapublishing.org/abstract.cfm?URI=josa-67-8-1105>.
- [48] Michael Watts. *A review of Optical Phased Array LiDAR*. 2018. URL: <https://www.youtube.com/watch?v=H-ZYe2IONOs> (visited on 06/18/2019).
- [49] P M Moser. *Spectral transmission of light through sea water*. Tech. rep. September. Pacific-Sierra Research Corporation, 1992. URL: <http://www.dtic.mil/docs/citations/AD1012965>.
- [50] T.M. Undeland N. Mohan and W. Robbins. *Power electronics*. 2003, p. 802.
- [51] S. Nakamura and M. Riordan. "The Dawn of Miniature Green Lasers". In: (2009).
- [52] Pep Lluis Negre, Francisco Bonin-Font, and Gabriel Oliver. "Cluster-based loop closing detection for underwater slam in feature-poor regions". In: *Proceedings - IEEE International Conference on Robotics and Automation*. Vol. 2016-June. IEEE, May 2016, pp. 2589–2595. ISBN: 9781467380263. DOI: 10.1109/ICRA.2016.7487416. URL: <http://ieeexplore.ieee.org/document/7487416/>.
- [53] Newton. *M310UW Dual Usage Laser Scanner*. URL: [https://www.newtonlabs.com/scan%7B%5C\\_%7Dm300uw%7B%5C\\_%7Dsys%7B%5C\\_%7Dspecs.html](https://www.newtonlabs.com/scan%7B%5C_%7Dm300uw%7B%5C_%7Dsys%7B%5C_%7Dspecs.html).
- [54] Nic Bingham. *Designing pressure-tolerant electronic systems*. 2013. URL: <https://www.uutech.com/ptepaper/> (visited on 07/12/2019).
- [55] R. Nowakowski and N. Tang. "Efficiency of synchronous versus nonsynchronous buck converters". In: (2009).
- [56] Takashi; Ogawa and Gerd; Wanielik. "FUSION 2016 : 19th International Conference on Information Fusion : proceedings : Heidelberg, 5-8 July 2016." In: (2016), p. 2337. URL: <https://ieeexplore-ieee-org.tudelft.idm.oclc.org/document/7528061>.
- [57] "Optical phased array lidar system and method of using same". In: (May 2014). URL: <https://patents.google.com/patent/US20160161600A1/en>.
- [58] Ouster. *Ouster Lidar product listing*. URL: <https://www.ouster.io/> (visited on 06/18/2019).
- [59] Bing Ouyang, Fraser R Dalglish, and Anni K Vuorenkoski. *Feasibility Study of Compressive Sensing Underwater Imaging Lidar*. 2014. URL: <https://apps.dtic.mil/docs/citations/ADA622707>.
- [60] Angus Pacala. *How Multi-Beam Flash LIDAR Works (Ouster blog)*. 2018. URL: <https://www.ouster.io/blog-posts/2018/11/8/how-multi-beam-flash-lidar-works> (visited on 06/18/2019).
- [61] Henry Plaessmann et al. "Multipass diode-pumped solid-state optical amplifier". In: 18.17 (1993), pp. 1420–1422.
- [62] Christopher V. Poulton et al. "Coherent solid-state LIDAR with silicon photonic optical phased arrays". In: *Optics Letters* 42.20 (2017), p. 4091. ISSN: 0146-9592. DOI: 10.1364/ol.42.004091.
- [63] Kraken Robotics. *The Kraken SeaVision: 3D RGB Underwater Laser Scanner*. URL: <https://krakenrobotics.com/products/seavision/>.
- [64] Matija Rossi et al. "Real-Time Underwater StereoFusion". In: *Sensors (Basel, Switzerland)* 18.11 (Nov. 2018), p. 3936. ISSN: 14248220. DOI: 10.3390/s18113936. URL: <http://www.mdpi.com/1424-8220/18/11/3936>.
- [65] S Rutten et al. "On the way to a pressure tolerant LiDAR for deep sea robot navigation". In: 4472659 ().
- [66] Davide Scaramuzza et al. "Past, Present, and Future of Simultaneous Localization and Mapping: Toward the Robust-Perception Age". In: *IEEE Transactions on Robotics* 32.6 (2016), pp. 1309–1332. ISSN: 1552-3098. DOI: 10.1109/tro.2016.2624754.
- [67] T. Schoedl and U.T. Schwarz. "Facet degradation of GaN heterostructure laser diodes". In: (2005).
- [68] David J. Segelstein. "The complex refractive index of water". In: (1981). URL: <https://mospace.umsystem.edu/xmlui/handle/10355/11599>.
- [69] Sexton Corporation. *Sexton camera enclosures*. URL: <http://www.thesextonco.com/shop/camera-enclosures/> (visited on 07/12/2019).
- [70] Yoni Sher et al. "Low Intensity LiDAR using Compressed Sensing and a Photon Number Resolving Detector". In: (Feb. 2018). arXiv: 1802.09354. URL: <http://arxiv.org/abs/1802.09354>.
- [71] *Side scan sonar, Klein Marine inc*. URL: <http://kleinmarinesystems.com/products/side-scan-sonar/>.
- [72] High Side and Current Monitor. "Supertex inc." In: 408 (), pp. 1–6.

- [73] Sidus Solutions LLC. *Cameras*. URL: <http://www.sidus-solutions.com/product-category/cameras/> (visited on 07/12/2019).
- [74] A E Siegman. "How to ( Maybe ) Measure Laser Beam Quality". In: d.October 1997 (1998), pp. 1–18.
- [75] Slamtec. *RPLIDAR S1 product listing*. URL: <https://www.slamtec.com/en/Lidar/S1> (visited on 06/18/2019).
- [76] Slamtec. *RPLIDAR-A1 product listing*. URL: <https://www.slamtec.com/en/Lidar/A1> (visited on 06/18/2019).
- [77] SOA (FPA and TWA) explanation. URL: <https://www.youtube.com/watch?v=t15RFzX11YU>.
- [78] Fiber Optics Solutions. *Semiconductor Optical Amplifier (SOA) Introduction*. 2017. URL: <http://www.fiber-optic-solutions.com/introduction-semiconductor-optical-amplifier-soa.html>.
- [79] R. Stevenson. *Lasers get the green light*. 2010. URL: <https://spectrum.ieee.org/semiconductors/optoelectronics/lasers-get-the-green-light>.
- [80] Sulis Subsea. *Sulis Z70*. 2016. URL: [http://www.sulissubsea.com/wp-content/uploads/2018/10/SULIS-Z70%7B%5C\\_%7Ddatasheet-20181029.pdf](http://www.sulissubsea.com/wp-content/uploads/2018/10/SULIS-Z70%7B%5C_%7Ddatasheet-20181029.pdf).
- [81] Ronald P Szumski and James K West. "United States Patent ( 19 )". In: 19 (1991).
- [82] *Teledyne technologies*. URL: <http://www.teledyne.com/>.
- [83] Texas Instruments Incorporated. *LIDAR Pulsed Time of Flight Reference Design*. 2018. URL: <http://www.ti.com/tool/TIDA-00663%7B%5C#%7Dtechnicaldocuments>.
- [84] Texas Instruments Incorporated. *LM5166 3-V to 65-V Input , 500-mA Synchronous Buck Converter With Ultra-Low I Q*. 2017.
- [85] Texas Instruments Incorporated. *Nanosecond Laser Driver Reference Design for LiDAR*. 2018. URL: <http://www.ti.com/tool/TIDA-01573%7B%5C#%7Dtechnicaldocuments>.
- [86] Texas Instruments Incorporated. *TL783 High-voltage Adjustable Regulator*. 2015.
- [87] A. R. Thurber et al. "Ecosystem function and services provided by the deep sea". In: *Biogeosciences* 11.14 (July 2014), pp. 3941–3963. ISSN: 17264189. DOI: 10.5194/bg-11-3941-2014. URL: <https://www.biogeosciences.net/11/3941/2014/>.
- [88] Timothy B. Lee. *Why spinning lidar sensors might be around for another decade*. 2018. URL: <https://arstechnica.com/cars/2018/05/why-bulky-spinning-lidar-sensors-might-be-around-for-another-decade/> (visited on 06/18/2019).
- [89] Tritech. *Gemini 720im Multibeam Sonar*. URL: <https://www.tritech.co.uk/product/gemini-720im>.
- [90] Velodyne. *Velodyne Puck product listing*. URL: <https://velodynelidar.com/vlp-16.html> (visited on 06/18/2019).
- [91] High-input Voltage. "LR8 High-Input Voltage, Adjustable, 3-Terminal, Linear Regulator". In: (2017), pp. 1–18.
- [92] Jim Williams. "Application Note 98 November 2004 Signal Sources , Conditioners and Power Circuitry AN98-1 Application Note 98 AN98-2". In: November (2004), pp. 1–28.
- [93] Amy Christine Wilson et al. "( 12 ) United States Patent". In: 2.12 (2016).
- [94] Huikai Xie et al. "Wide-angle structured light with a scanning MEMS mirror in liquid". In: *Optics Express* 24.4 (2016), p. 3479. DOI: 10.1364/oe.24.003479.
- [95] Fangpei Zhang. "Broad band direct modulation for chirp AM lidar". In: *Optik* 130 (Feb. 2017), pp. 383–392. ISSN: 00304026. DOI: 10.1016/j.ijleo.2016.10.097. URL: <https://www-sciencedirect-com.tudelft.idm.oclc.org/science/article/pii/S0030402616312475>.
- [96] Hao Zhang et al. "Bidirectional reflectance measurements of sediments in the vicinity of Lee Stocking Island, Bahamas". In: *Limnology and Oceanography* 48.1part2 (Jan. 2003), pp. 380–389. ISSN: 00243590. DOI: 10.4319/lo.2003.48.1\_part\_2.0380. URL: [http://doi.wiley.com/10.4319/lo.2003.48.1%7B%5C\\_%7Dpart%7B%5C\\_%7D2.0380](http://doi.wiley.com/10.4319/lo.2003.48.1%7B%5C_%7Dpart%7B%5C_%7D2.0380).
- [97] Xiaoyang Zhang et al. "MEMS mirrors submerged in liquid for wide-angle scanning". In: *2015 Transducers - 2015 18th International Conference on Solid-State Sensors, Actuators and Microsystems, TRANSDUCERS 2015* (2015), pp. 847–850. DOI: 10.1109/TRANSDUCERS.2015.7181056.
- [98] □□□□□□□□□□□□□□. *Laser radar based on MEMS micro mirror*. Nov. 2015. URL: <https://patents.google.com/patent/CN205120965U/en?q=lidar+mems>.



# Appendix

## A.1. Matlab script for range estimation

```
%% define some symbols
syms distance
assume(distance, 'positive')

%% system specs
% transmission specs
slope_efficiency.min = 0.6; % W/A
slope_efficiency.max = slope_efficiency.min; % W/A

transmit_current.min = 1; % A
transmit_current.max = 1; % A

% detector specs
effective_area.min = 8e-3 * 17e-3; % m^2
effective_area.max = 8e-3 * 17e-3; % m^2

detector_threshold_current.min = 0.4e-6; % A
detector_threshold_current.max = 0.4e-6; % A

detector_efficiency.min = 8; % A/W
detector_efficiency.max = 8; %0.25; % A/W

% efficiencies
angular_efficiency.min = cos(deg2rad(75 / 4)) * 0.4;
angular_efficiency.max = 1;

hole_efficiency.min = 0.95;
hole_efficiency.max = 0.95;

optical_efficiency.min = 0.9;
optical_efficiency.max = 0.9;

% target specs
albedo.min = 0.1;
albedo.max = 0.2;

% medium specs
water_transmission.min = 0.95; % Np/m
water_transmission.max = 0.95; % Np/m

%% find rx current
```

```

efficiency.min = angular_efficiency.min * hole_efficiency.min * ...
                optical_efficiency.min;
efficiency.max = angular_efficiency.max * hole_efficiency.max * ...
                optical_efficiency.max;

medium_transmission.min = water_transmission.min^(2*distance);
medium_transmission.max = water_transmission.max^(2*distance);

% assumes lambertian full reflectance
spread.min = effective_area.min / (2 * pi * distance^2);
spread.max = effective_area.max / (2 * pi * distance^2);

transmission.min = efficiency.min * medium_transmission.min * spread.min * albedo.min
;
transmission.max = efficiency.max * medium_transmission.max * spread.max * albedo.max
;

tx_power.min = transmit_current.min * slope_efficiency.min;
tx_power.max = transmit_current.max * slope_efficiency.max;

rx_power.min = transmission.min * tx_power.min;
rx_power.max = transmission.max * tx_power.max;

rx_current.min = rx_power.min * detector_efficiency.min;
rx_current.max = rx_power.max * detector_efficiency.max;

%% find distance
expected_distance.min = vpasolve(rx_current.min == detector_threshold_current.max,
    distance, 0.1);
expected_distance.max = vpasolve(rx_current.max == detector_threshold_current.min,
    distance, 0.1);

expected_distance.min
expected_distance.max

```

## A.2. Transmission field integral

Assume a perfectly collimated beam travelling through a medium. Then for a length element  $\Delta\ell$  of constant transmissivity  $T$  we find that the intensity  $I$ :

$$I(\vec{R} + \vec{\Delta\ell}) = I(\vec{R}) \cdot T^{\Delta\ell} = I(\vec{R}) \cdot e^{\ln(T) \cdot \Delta\ell}$$

So for a path divided in  $N$  length elements of length  $\Delta\ell$  of constant transmissivity:

$$I(\vec{R} + \vec{P}(N)) = I(\vec{R}) \cdot \prod_{n=0}^{N-1} T(n)^{\Delta\ell} = I(\vec{R}) \cdot e^{\sum_{n=0}^{N-1} \ln(T(n)) \cdot \Delta\ell}$$

Taking  $N \rightarrow \infty$  yields:

$$I(\vec{b}) = I(\vec{a}) \cdot \exp\left(\int_{\vec{a}}^{\vec{b}} \ln(T(\vec{R})) \cdot |d\vec{R}|\right)$$

## A.3. The polygon

In the greenlight assessment, the question was raised if the angle of the shaft can be linearly interpolated.

The situation is displayed in figure A.1. The following parameters can be defined.

$$\mathbf{a} = \begin{bmatrix} r \sin(\phi) \\ -r \cos(\phi) \end{bmatrix} \quad \mathbf{b} = \begin{bmatrix} r \sin(\phi - \frac{\pi}{4}) \\ -r \cos(\phi - \frac{\pi}{4}) \end{bmatrix}$$

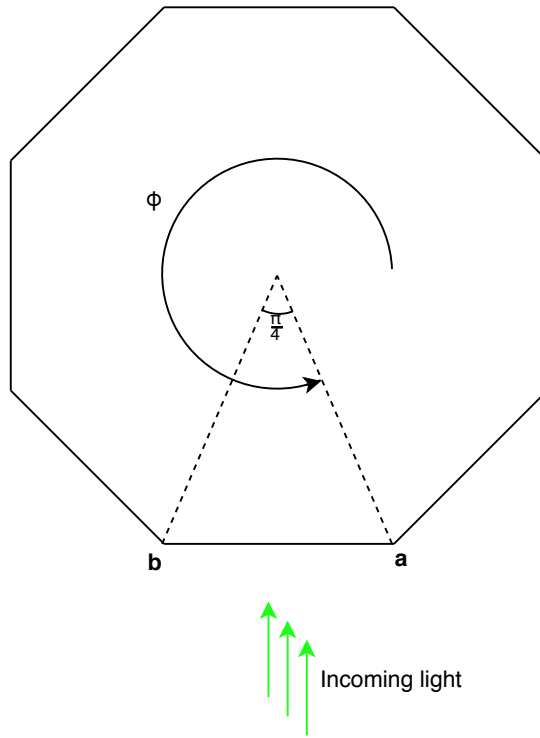


Figure A.1: Simplification of situation to prove angle can be linearly interpolated.

$$\|\mathbf{a}\| = \|\mathbf{b}\| = r$$

$$\mathbf{ab} = \mathbf{b} - \mathbf{a} = \begin{bmatrix} b_x - a_x \\ b_y - a_y \end{bmatrix}$$

Due to symmetry

$$0 \leq \phi \leq \frac{\pi}{4}$$

the normal vector  $\hat{n}$  is  $\mathbf{ab}$  shifted by 90 degrees and normalised

$$\hat{n} = \frac{1}{\|\mathbf{b} - \mathbf{a}\|} \begin{bmatrix} a_y - b_y \\ b_x - a_x \end{bmatrix}$$

Because the laser and the centre of the polygon are both in the y-z plane, the incoming light can be modeled as

$$r_i = \begin{bmatrix} 0 \\ 1 \end{bmatrix}$$

$r_o$  is the reflection vector of  $r_i$  over  $\hat{n}$

$$r_o = (r_i - \text{proj}_{\hat{n}}(r_i)) - \text{proj}_{\hat{n}}(r_i) = r_i - 2\hat{n}(\hat{n} \cdot r_i)$$

$$r_o = \begin{bmatrix} 0 \\ 1 \end{bmatrix} + \frac{2a_x - 2b_x}{\|\mathbf{b} - \mathbf{a}\|^2} \begin{bmatrix} a_y - b_y \\ b_x - a_x \end{bmatrix}$$

$$\|\mathbf{b} - \mathbf{a}\|^2 = (b_x - a_x)^2 + (b_y - a_y)^2$$

so

$$r_o = \begin{bmatrix} 0 \\ 1 \end{bmatrix} + \frac{2a_x - 2b_x}{(b_x - a_x)^2 + (b_y - a_y)^2} \begin{bmatrix} a_y - b_y \\ b_x - a_x \end{bmatrix}$$

Substituting and simplifying gives

$$r_0 = \begin{bmatrix} -\cos(2\phi + \frac{\pi}{4}) \\ -\sin(2\phi + \frac{\pi}{4}) \end{bmatrix} = \begin{bmatrix} \cos(2\phi + \frac{5\pi}{4}) \\ \sin(2\phi + \frac{5\pi}{4}) \end{bmatrix}$$

Clearly, the angle of the reflection is  $2\phi + \frac{5\pi}{4}$  with respect to the x-axis. This means that the angle of the reflected light is linear with  $\phi$  and thus can be linearly interpolated. From this the Field Of View (FOV) can be derived. Because the domain was specified as  $0 \leq \phi \leq \frac{\pi}{4}$ , the horizontal FOV is  $90^\circ$ . It was also known that the vertical angle from one plane to the next differs  $4.5^\circ$ . This means that the vertical FOV is  $36^\circ$ . Unfortunately, this does not meet *shall* requirement PER5-a, but it complies with the minimal PER5-b requirement.

## A.4. Beam divergence

Beam divergence is characterized as the increase in the beam diameter when propagating through space. This characteristic is important to determine the feasibility of focusing a light source into a collimated beam. Figure A.2 illustrates this beam characteristic of a light source.

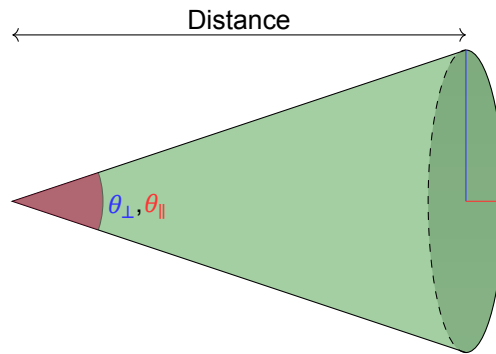


Figure A.2: This figure illustrates the beam divergence characteristic parallel and perpendicular to the pn-junction of the laser diode. The beam divergence of a laser beam scales proportionally with the propagating distance

In the figure above, the beam divergence is characterised by the parallel and perpendicular angle and this angle varies with each light source.

## A.5. Laser

For the design of the LiDAR, a laser was chosen as it will provide high optical output power and the optical power is mostly concentrated in the laser beam. The types of lasers that were taken into consideration are as follow :

- Gas laser [2]  
This type of laser consist of current discharging through a gas, whether it be Helium or Carbon-dioxide gas, to produce a laser signal. While all the gas atoms are being excited by the forward current, a coherent light is produced and exits through a lens. The main advantage of gas lasers is its high efficiency.
- Semiconductor laser [2]  
A semiconductor laser, or more commonly known as laser diode, is a type of laser which uses a semiconductor for excitation. The laser beam is created at the laser's junction. The wavelength (or the colour) of the laser beam is dependent on the material of the semiconductor. This type of laser is very common as this type of laser has wide variety of applications. Other advantages of this type of laser is its ease of use, high efficiency, low power consumption and long lifetime. Another advantage that should be elaborated upon is the high modulation frequency of a laser diode. The laser diode has a characteristic that whenever there is a variation of the injection current then there is a variation of the optical emission variation. From this it can be said that modulation bandwidth frequency can be higher than the MHz region.
- Liquid laser [2]  
The liquid laser, or more commonly know as dye laser, is a type of laser in which the gain medium is in liquid form. The material of the gain medium is made of liquid organic dye which is dissolved in liquid solvents. The main advantage of dye lasers is the wide range of wavelength it can produce from its medium.
- Fiber laser [25]  
This type of laser is comprised of a gain medium that is optically doped with fiber. The main advantage of this

type of laser is the fact that it produces a high beam quality, while also having a high optical output power. Beam quality is meant in this context the measured beam characteristics compared to an ideal beam quality, which is the gaussian beam. A gaussian beam is a beam signal, where the electric and magnetic field amplitudes are profiled by the gaussian function. Thus a high beam quality means that the measured beam signal approaches the gaussian beam characteristics [74].

For LiDAR applications, the type of lasers used vary with each LiDAR system. Yet the most commonly used laser within a LiDAR system is the laser diode, this due to the fact that this implementation provide relatively higher optical output power while operating at a lower electrical power level. For bigger LiDAR systems, the laser diodes are more appealing to use as multiple laser diodes can be easily attached onto an array.

In patent [93], a laser diode is used for the needs of the transmission stage and multiple laser diode are used for the pulse LiDAR system. The only difference is is that the wavelength of the laser diode is around 905 nm. In another patent [81], a laser diode is used in the wavelength region of around 805 nm and the operating modulation frequency is around 80 MHz for the flash LiDAR system. For both of these patent, the reason for the use of laser diode instead of other types of lasers is relatively unknown, as no concrete reason is given as to why a laser diode is used in the LiDAR system.

It is worth noting that the type of laser diodes used in LiDAR systems are different from the conventional laser diodes. Conventional laser diodes have lower optical power, this value can be around few milli Watts as this can be used by the general public without causing too much damage to a person's eye. While the laser diodes used in LiDAR systems must have a high optical power in order to minimise the error margin and to achieve a higher range.

## A.6. Optical Amplifiers

Optical amplifiers are, what the name entails, amplifiers to amplify an optical signal without first converting the optical signal into an electrical signal for amplification. There is however an electrical current that is pumped through these amplifiers to ensure that the optical output power is increased. This type of amplifier can be used to amplify the optical signal from the transmission stage of the LiDAR system, this will ensure that the error margin of the received signal is smaller as the optical output power is increased. There are several optical amplifiers that were taken into consideration for the design of the LiDAR and they are listed as follow:

- Semiconductor Optical Amplifier [78]

This type of optical amplifier uses a semiconductor to amplify the optical signal. The basic principle of this type of optical amplifier is the input signal goes through the active region of the semiconductor, in the active region there is a current pumped through the active region. In the active region photons are released and because the photons have the same wavelength as the optical input signal, the signal is thus amplified. There are two types of Semiconductor Optical Amplifier, the Fabry-Pérot Amplifier and the Travelling Wave Amplifier.

- Fabry-Pérot Amplifier [77]

The Fabry-Pérot amplifier consist of a semiconductor and two reflective mirrors at each end of the semiconductor. When the input signal enters the active region of the semiconductor, it will reflect back and forth between the mirrors and thus will amplify the optical output power. Analysing the magnitude response of this amplifier illustrates an alternating response in which a frequency range could be either attenuated or amplified. The main issue with this amplifier, is the fact a certain frequency range can be greatly amplified or attenuated, this makes the decision of choosing a specific operating modulation frequency range more challenging. On the other hand, this can be seen as an advantage as generated noise frequencies can be attenuated and only a specific frequency range is amplified. Another disadvantage of this type of optical amplifier, is the sensitivity for higher frequencies.

- Travelling Wave Amplifier [77]

The Travelling Wave amplifier has the same basic principle as the Fabry-Pérot amplifier, but the input signal is amplified during one pass through the active region of the semiconductor. This ensures that the magnitude response of this type of amplifier is uniform for a large frequency band, ensure for a higher optical bandwidth. One drawback of this type of amplifier is that maximum achievable gain of this type of amplifier does not exceed that of the Fabry-Pérot variant.

These amplifiers are implemented in what is called a MOPA configuration. MOPA configuration is a type of configuration that is mainly used to house and facilitate the optical amplifier and the source. MOPA stands for Master Oscillator Power Amplifier and this type of configuration is commonly used for amplification of an optical signal.

- Erbium Doped Fiber Amplifier [22]

How this type of amplifier operate is that it uses pump wavelengths to go from one excited state to another excited state, this occurs when the Erbium ions absorb the incoming light. Pump wavelengths are meant within

this context as external wavelengths that are essentially pumped into the input stage of EDFA along with the input laser signal, their purpose is to ionize the Erbium ions from one state to the other state in which the emitted wavelength is around the same wavelength as the laser signal. While the signal goes from the one state and the other, the signal is thus amplified. The main issue with the Erbium Doped Fiber Amplifier (EDFA) is that it requires a large device and the fiber wires used requires to be at least several kilometers long.

- Tapered Amplifier [17]

This type of amplifier is comprised out of a two parts. The first part is the the ridge section, which ensures high beam quality. The second part is the taper section, this ensures that the optical output power is increased when the length of the taper section is increased. How the amplification occurs within the tapered section is explained as follow

1. The tapered section of the amplifier is externally pumped by a current source and the tapered section consist of a gain medium
2. When the laser signal goes through the ridge section and into the tapered section, the laser signal diffracts completely and will fill up the gain medium of the tapered section
3. As the externally pumped current source provides enough power, the laser signal is thus amplified.

The type of setup for this type amplifier is usually a lens that corrects the output optical signal, as this signal diverges after being amplified by this amplifier.

- Solid state amplifier [61]

This type of amplifier uses a wide variety of doped materials (mostly a crystal) in different shapes, whether it be a disk shape or square shape, to amplify the optical output signal. The working of this amplifier is as follow, the laser signal comes into the input stage of the crystal. There the laser signal is reflected within the crystal to the gain medium of the crystal, the gain medium is externally pumped by electrical power hence the reason as to how during the first reflection the laser signal is amplified. Then the amplified laser signal is reflected within the crystal once again, where it would once again reach the gain medium of the crystal. During this photon recombination will occur. This process will continue while the amplified laser signal exits through a lens and into the free space. This type of amplifier does ensure that the wavelength of the outgoing optical signal is different from the incoming optical signal, this is due to the photon recombination.

Further research as to how an optical amplifier is implemented within a LiDAR system showed little results. Yet in patent [18] illustrated a LiDAR system where a EDFA is implemented in Master Oscillator Power Amplifier (MOPA) configuration to achieve a optical output power greater than 1 W. While in airborne LiDAR system, an Nd:YAG solid state amplifier is used. Nd:YAG stands for neodymium-doped yttrium aluminum garnet, which is the material used for the gain medium.

## A.7. Laser driver of TI test results

The laser driver has a waveform which is some what longer than 100 ns, otherwise no pulse would be created. This already shows that the laser driver is very unstable, a small change in pulse width could result in no pulse. Next the voltage of the incoming pulse was decreased from 5.124 V to 5.04 V, which as Figure A.3 and Figure A.4 showed a significant change in the outgoing pulse.

## A.8. Diodes

Diodes experience recovery time, this is due to the flow of minority carries that can not be stopped or started immediately. Schottky diodes however do not experience this, since they are not constructed from two semiconductor junctions like pn-diodes. They are formed from a thin film of metal adjacent to a semiconductor material, due to this difference in construction the Schottky diode has a faster turn-on and turn-off time. The exact physics behind this phenomenon is not important, but in short Schottky diode are majority-carrier devices and do not have stored minority carries while pn-diode do. Schottky diodes however do have a large space charge capacitance, as much as a factor of 5. This is due to the fact that the depletion region of a Schottky diode is much smaller, because of the heavier doping used in the semiconductor material [50]. The depletion region width is related to the capacitance as  $C = \epsilon \frac{A}{d}$ . Therefore even with a Schottky diode the possibility of generating a secondary pulse is a real outcome.

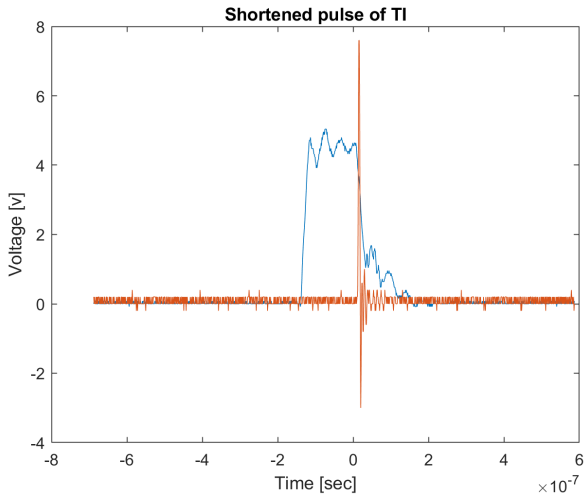


Figure A.3: With a voltage of 5.124V

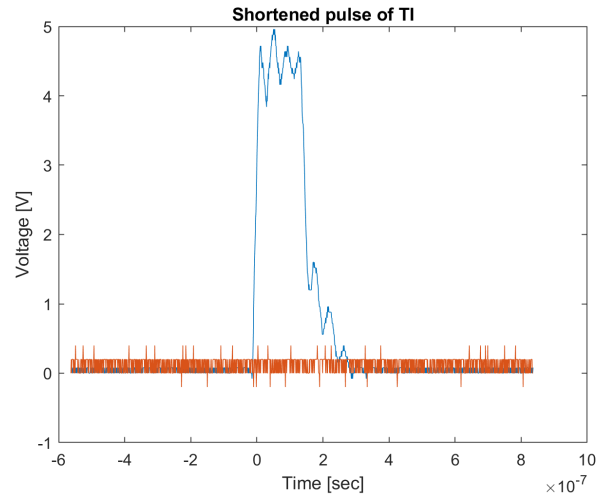


Figure A.4: With a voltage of 5.04V

## A.9. Power converters

Power electronic converters are needed to convert the 48 V to multiple power levels, namely for the APD bias voltage, the bus voltage and bias voltage of the laser driver. The APD reverse bias will require a step-up converter, the bus voltage can either be a step-up or a step-down depending on the maximum voltage level that the laser diode can handle and the bias voltage for the laser driver requires a step-down converter. Therefore multiple power converters were researched. These are discussed in the following sections and in the next chapter the choice of power converter for each of the three systems is made based on the advantages and disadvantages mentioned here.

There are multiple DC-DC converters which can be divided into three categories: linear mode, switch mode and resonant mode. The main difference between each mode is the efficiency and the complexity of the control circuitry. Figure A.5 gives an overview of all the possible topologies for each of the modes. Each converter category will now briefly be discussed.

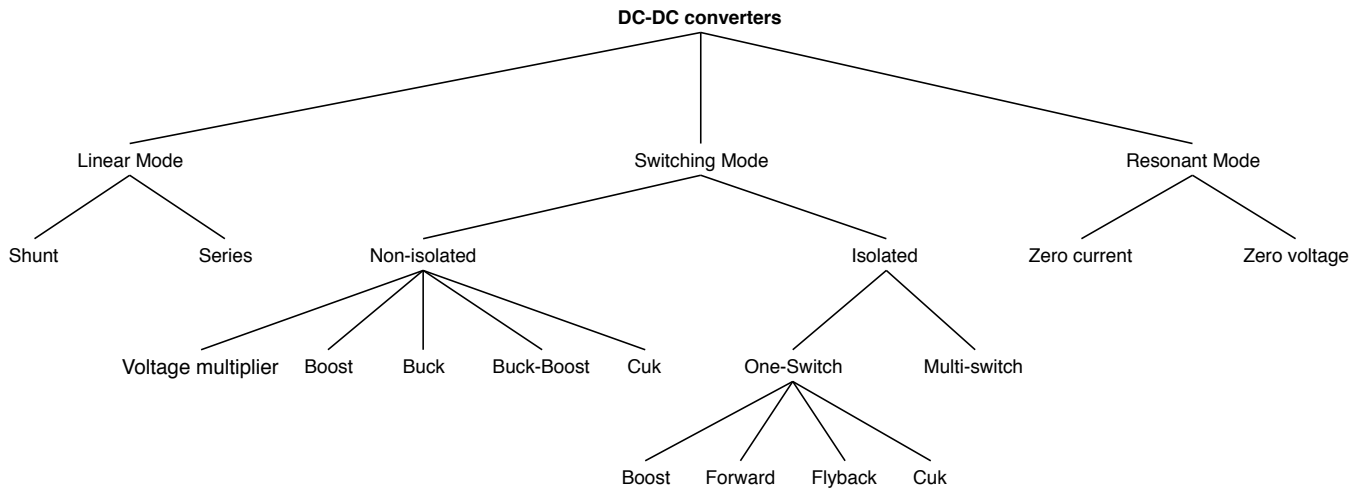


Figure A.5: Power converter tree based on [Power converter tree]

### A.9.1. Linear mode

Linear converters or also called linear regulators create a constant voltage output by operating a pass device in the linear region, which causes it to behave like a controllable variable resistor. The pass device is controlled by a error amplifier, which compares the output voltage with a reference voltage and generates a control signal accordingly. There are two important aspects of a linear regulator that determine whether this device can be used for a certain application as explained below.

- In order to regulate the output voltage the difference between the input and output voltage must be greater than the dropout voltage. Otherwise, the resistance of the pass device will be too low and the output can not be

regulated. This means that the linear regulator can only be used as a step-down converter with a minimum voltage difference between the input and output of  $V_{drop}$  [36].

- The power dissipation of linear regulators can be described by the power dissipated through the variable resistance, which equals  $P_{diss} = (V_{in} - V_{out})I_{out}$  when the ground current is neglected. From this the efficiency can be described by  $\eta = \frac{V_{out}}{V_{in}} * 100\%$ .

Linear regulators are inefficient when compared to other converters and due to the high power dissipation they are often in need of a heat sink, which makes the circuitry a lot larger. Apart from these disadvantages, the control circuitry of a linear regulator is less complicated and the output voltage can easily be made adjustable. From these aspects follow the main advantages and disadvantage of a linear mode converter, these are listed below. It must be mentioned that when the difference between the input voltage and output voltage remains low and the output current is also small, linear regulators are good options to use due to their simplicity.

- |                                    |   |
|------------------------------------|---|
| + Simple circuitry                 | – Only step-down conversion                       |
| + Simple adjustable output voltage | – Inefficient, $\frac{V_{out}}{V_{in}}$           |
| + Low part count                   | – Thermal dissipation is high                     |
| + Low noise                        | – Heat sink often necessary, thus large footprint |

### A.9.2. Switching mode

Switching mode converters convert the input voltage by operating an active device as a switch at a high frequency, causing a constant average output voltage. As Figure A.5 shows, there are two switch mode topologies, isolated and non-isolated. Isolated topologies use a transformer to decouple the input from the output, these topologies are often required due to safety reasons. The extra isolation is an added modification to the non-isolated topologies. Therefore only the non-isolated converters will be discussed.

The buck and boost converter are basic converter topologies, with the buck being a step-down converter and the boost a step-up converter. The buck-boost and cuk converters have inverter topologies and are combinations of these two basic converters. Since they are a combination of a buck and boost converter together the output voltage can either be lower or higher than the input voltage. Such an output voltage range is not needed in our system, therefore these topologies have not been considered.

There are two buck and boost converter configurations; synchronous and asynchronous. The structural difference is that asynchronous uses a diode as low side switch, while in a synchronous circuit this has been replaced with a transistor. The transistor is turned on or off in operation opposite from the high side switching element. The working principle of both circuit is the same, the difference is seen when comparing efficiency.

In the case of a buck converter it is assumed that synchronous buck converters have better efficiency. Since the equivalent forward-voltage drop over the diode is considerably less when replacing it with a MOSFET. This drop contributes to the overall loss of the converter in the form of a product of the forward-voltage drop and forward-conduction current [41]. The voltage drop is lower when using a MOSFET due to the fact that the MOSFET has a low on-resistance, therefore there are lower ohmic losses. At higher currents, the drop across the MOSFET's on-resistance can however be higher than that of a diode. This is normally solved by placing more MOSFETs in parallel.

Even though the voltage-drop will be lower when using a MOSFET, a study comparing both converters shows that non-synchronous buck converters operate with a higher efficiency at light load applications [55]. The same study also compares the costs and size of each converter, it concludes that synchronous converters will be smaller and might be more cost efficient when compared to the non-synchronous converter. Both topologies must be considered when implementing a buck or boost converter. The decision for which topologies is dependent on the application.

In order to be able to compare the switching converter with the others, the overall advantages and disadvantages are given in the list below.

- |   |                             |
|---|-----------------------------|
| + Efficiency, 60-90%                                  | – Medium part count         |
| + Step-up, Step-down and Step-up-Step-down conversion | – Switching noise           |
|   | – Medium circuit complexity |

### A.9.3. Resonant mode

The resonant mode converters were designed as an improvement of switching mode converters. Switching mode converters are required to turn off and on the full load current during each switch. This causes the switches to be subjected to high switching stress and high switching power losses, which increase with increasing switching frequency. Increasing the switching frequency allows for a smaller and often cheaper converter, due to smaller inductors and capacitors. The switching stress can often be limited by using a snubber circuit, a circuit consisting of diodes and passive components placed in series or parallel with the switches [50]. Snubbers however do not decrease the switching power losses, these losses are now shifted from the switch to the snubber circuit.

Resonant mode converters significantly reduce the switching power loss by only turn on or off the switches when either the switch voltage is zero or the switch current is zero. There are multiple converter topologies, which form a combination of the proper converter with the right switching strategy. The complexity of each topology is however very high.

These advantages and disadvantages of the resonant mode converter are summed up below.

- + Low switching losses
- + Very high efficiency
- + High switching frequency, small footprint
- High circuit complexity

### A.10. APD boost converter

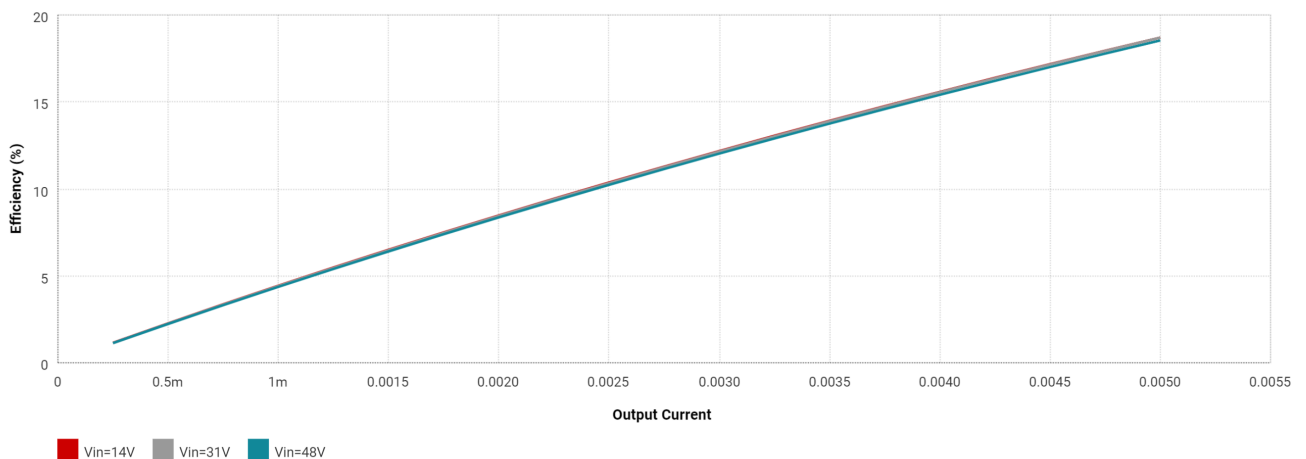


Figure A.6: Efficiency of a Quasi-resonant converter with 130V output at 5 mA load current

### A.11. Pulse generator simulation

Here the simulation of the pulse generator is given, with a difference in resistance of  $170 \Omega$ . This gives approximately a pulse width of  $1 \text{ ns}$ , which confirms the working of the design.

### A.12. Explanation of the frequency doubling [10]

As the incoming optical wave enters the crystal structure, the photons will interact with one another and will recombine into one single photon which has twice the amount of energy but double the frequency and thus half of the original wavelength. Recombination of the two photons is illustrated in figure A.8, a cumulative transition between 2 states will result into one big transition from the final state back to the ground state. From this final transition a new photon is generated with a frequency, which is two times higher than that of the incoming optical signal. The resulting optical wave is a nonlinear polarization wave, this is due to the nonlinearity of the crystal. Due to this characteristic, a phenomena occurs which is called phase mismatch. Phase mismatch is the occurrence where the wavenumber of the resulting wave is higher than that of the incoming wave, this occurs as the phase velocity is frequency dependant on the medium. Equation A.1 which shows this relation and figure A.9 depicts the phase mismatch phenomena with  $\Delta k$  being the phase mismatch.

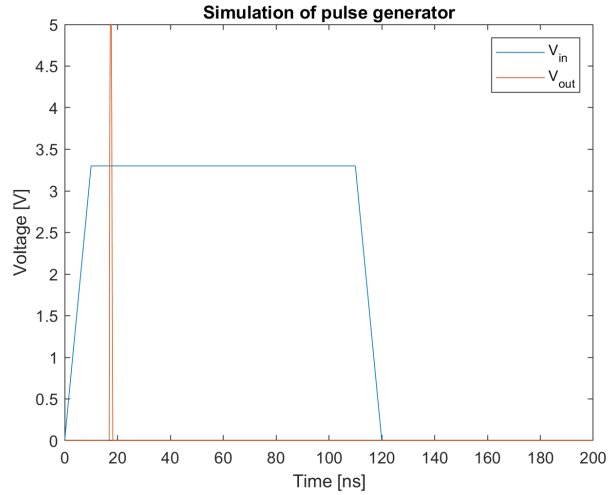


Figure A.7: Simulation of pulse generator

$$v = \frac{c_0}{n} \quad (\text{A.1})$$

In equation A.1,  $v$  is the phase velocity,  $c_0$  is the speed of light which is  $299\,792\,458\text{ m s}^{-1}$  and  $n$  is the refractive index of the medium. As there is phase mismatch in the medium, the overall efficiency of the conversion of the frequency decreases. Equation A.2 shows the relation between phase mismatch and the efficiency of the conversion.

$$\eta = \frac{I_{out}}{I_{out}^{max}} = \text{sinc}(\Delta k L / 2)^2 \quad (\text{A.2})$$

Here the phase mismatch is given as  $\Delta k$  and  $L$  is the length of the crystal. To increase efficiency of the conversion, one might look into the possibility of different crystals made up of different materials. This may be a solution, as the different materials have different refractive indexes and thus the most optimal material of a crystal can be chosen. Another solution may be to tune the length of the crystal, in order to avoid phase mismatch completely. Lastly, the angle at which the incoming optical signal is directed can be tuned to achieve a proper optical output, as the angle of the incoming changes the phase mismatch characteristics changes [30, p. 269]. Although phase mismatch plays a huge role in determining the efficiency of the conversion, there are of course other factors where the efficiency could decrease like temperature [7]. These factors may be the effective area of the crystal and the effective nonlinearity of the crystal, equation A.3 illustrates complete description of the output optical intensity.

$$I_{out} = \frac{8d_{eff}^2\omega_{out}^2I_{in}^2}{n_1^2n_2\epsilon_0c^2}L^2\text{sinc}(\Delta k L / 2)^2 \quad (\text{A.3})$$

Here  $d_{eff}$  is the nonlinear coefficient of the crystal and  $n_i$  is refractive index of the given optical signal. Frequency doubling crystals in the market that were considered for implementation were KTP (Potassium titanyl phosphate), LBO (Lithium triborate) and BBO (Beta barium borate) crystals. While it assumed that one crystal should suffice with the conversion of the wavelength of the incoming optical signal, in most practical cases this is not the case. In most topologies of laser systems with a frequency doubling crystal, a solid state optical amplifier is mounted between the infrared laser diode and the frequency doubling crystal. This will not only amplify the optical signal, but also convert the wavelength of the signal to a higher wavelength, as already explained in appendix A.6. An example of such implementation can be seen in [79], where a ND:YAG solid state amplifier is used to convert the wavelength of the infrared laser diode to a wavelength of 1064 nm. The now converted optical signal will then propagate through the frequency doubling crystal, which will then result to a output optical signal with a wavelength of 532 nm.

Although the implementation of a frequency doubling crystal shows a lot of promise, it does not have a 100 % conversion efficiency. To tune the conversion efficiency to an acceptable level requires more background information about nonlinear optics. This is unfortunately not feasible within the timespan of the project, but the concept for the design of a laser diode with a frequency doubling crystal should be considered for future optimizations of the transmission stage.

### A.13. Derivation for the component values for the buck converter, Bias voltage

In this section, the derivation for each component value for the buck converter is thoroughly discussed and documented. These component values were derived according to the operating conditions discussed in the datasheet of

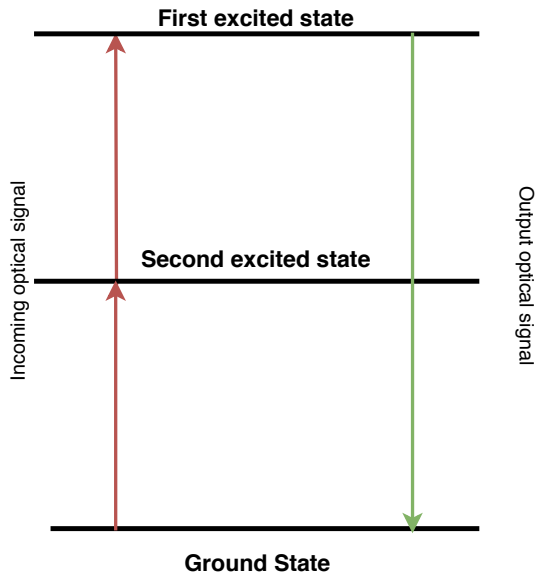


Figure A.8: Recombination of two photons will result in a single photon with a higher energy level

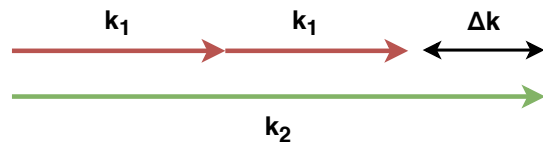


Figure A.9: Figure depicting the phase mismatch phenomena.  $\Delta k$  is the phase difference between the phase of the incoming and the outgoing optical signal

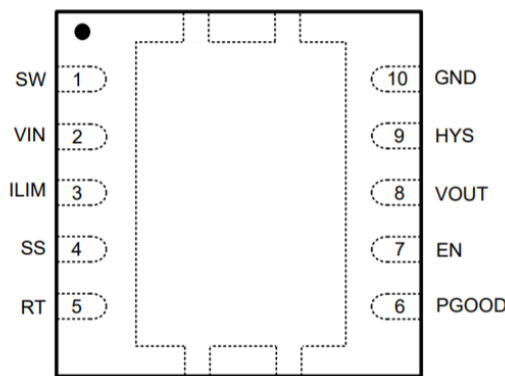


Figure A.10: Pinout of the LM5166 buck converter

the LM5166 IC [84]. Figure A.10 depicts the pinout of the LM5166 IC.

### A.13.1. VIN and EN pin

The VIN pin is the input voltage connection and can withstand a maximum 65 V input voltage. For this pin, it was recommended in the datasheet to connect a 2.2  $\mu\text{F}$  in parallel with the VIN pin.

The EN pin is the enable pin of the converter. The converter is turned on when the voltage at the pin is greater 1.2 V, thus it was decided to connect this pin to the VIN pin as the maximum voltage at the EN pin is 65 V.

### A.13.2. PGOOD pin

The PGOOD pin is the flag pin to indicate whether the output voltage is within a regulation window. This pin is used whenever multiple converter are daisy chained to each other. As only one buck converter is used, it was decided to leave this pin floating.

### A.13.3. SS pin

The SS pin is the enable the soft start of the buck converter. This pin can be programmed to use the soft start or not, but to ensure proper functioning of the buck converter at all times a 33 nF capacitor is connected to the SS pin to

enable soft start.

#### A.13.4. RT pin

The RT pin is a programmable pin which indicates whether the buck converter operates in constant on time mode or pulse frequency modulation mode. Pulse frequency modulation mode ensures the voltage coming from the SW pin has an active and a sleep period, while the constant on time mode ensures the voltage coming from the SW pin is adjusted based on the input voltage and the set output voltage. While both modes have their advantages, it was decided to implement the pulse frequency modulation mode for the sake of simplicity and thus the RT pin is connected to ground.

#### A.13.5. HYS pin

The HYS pin is a programmable to ensure a customizable hysteresis is set for an undervoltage lockout. Since it is assumed that an undervoltage event will not occur under any circumstances, the HYS pin is thus connected to ground.

#### A.13.6. SW pin

The SW pin is the switching node of the buck converter. At this node the buck inductor is connected. The inductance value is calculated as per equation A.4.

$$L = \frac{V_{out}}{f_{sw}^{max}} \cdot \left(1 - \frac{V_{out}}{V_{in}}\right) \quad (A.4)$$

Since the switching frequency can have an arbitrary value, it was decided to implement a switching frequency of 800 kHz. Furthermore, it was decided that the circuit should not supply a high current at the output. Thus it was decided that the circuit should supply a current of 0.2 A, this was programmed using the ILIM pin which is further elaborated in the next section. From this, the inductance value was derived:

$$L = \frac{6}{800000 \cdot 0.2} \cdot \left(1 - \frac{6}{48}\right) \approx 33\mu\text{H} \quad (A.5)$$

Thus an inductor with the value of 33  $\mu\text{H}$  was chosen.

#### A.13.7. ILIM pin

The ILIM pin is a programmable pin which ensures that the output current is limited to certain current level. As already in the previous section, the output current should have a maximum value of 200 mA. In the datasheet, it is mentioned that a resistor with a minimum value of 100 k $\Omega$  should be connected to the ILIM pin, in order to program the output current to have a maximum value of 200 mA. Therefore, a 105 k $\Omega$  was chosen to be connected to the ILIM pin.

#### A.13.8. VOUT pin

The VOUT pin is a programmable pin which sets the output voltage of the buck converter. The output voltage (6 V) is set using a resistor network that is connected to the VOUT pin. Equation A.6 depicts the equation used to calculate the resistor values of the resistor network.

$$R_{fbt} = \frac{1.223}{V_{out} - 1.223} \cdot R_{fbb} \approx 0.256R_{fbb} \quad (A.6)$$

From this ratio between the two resistor in the resistor network, it was decided to chose a 124 k $\Omega$  and 487 k $\Omega$  for  $R_{fbt}$  and  $R_{fbb}$  respectively.

### A.14. Derivation of the component values for the linear regulator, Bus voltage

In this chapter, the derived and eventual chosen component values are discussed and documented.

### A.14.1. Requirements

To first start the design of the linear regulator, one must list all of the requirements in order to derive the most optimal components values. Knowing the requirement for the voltage levels (as per section 4.5.1) and the operation conditions of the TL783 linear regulator, the requirements can be listed as follow.

1. As already stated before, the voltage range should be between 10 to 30 V.
2. As the datasheet of TL783 [86] states, the minimum output current should be 15 mA.

### A.14.2. Resistor network

To achieve a tunable voltage range of 10 to 25 V, one must use a potentiometer to achieve this. Given the voltage at the ADJ pin is typically 1.25 V, the output voltage can be set as follow.

$$V_{out} = 1.25 \left( 1 + \frac{R2 + R3}{R1} \right) \quad (A.7)$$

This due to the fact that a resistor network is set at the ADJ pin of the regulator, which is then indirectly connected to the OUT pin of the regulator. Figure A.11 depicts the resistor network needed between the two pins of the regulator. R1 and R2 are set resistor values and R3 is a potentiometer. Knowing the set requirement, the resistor values were

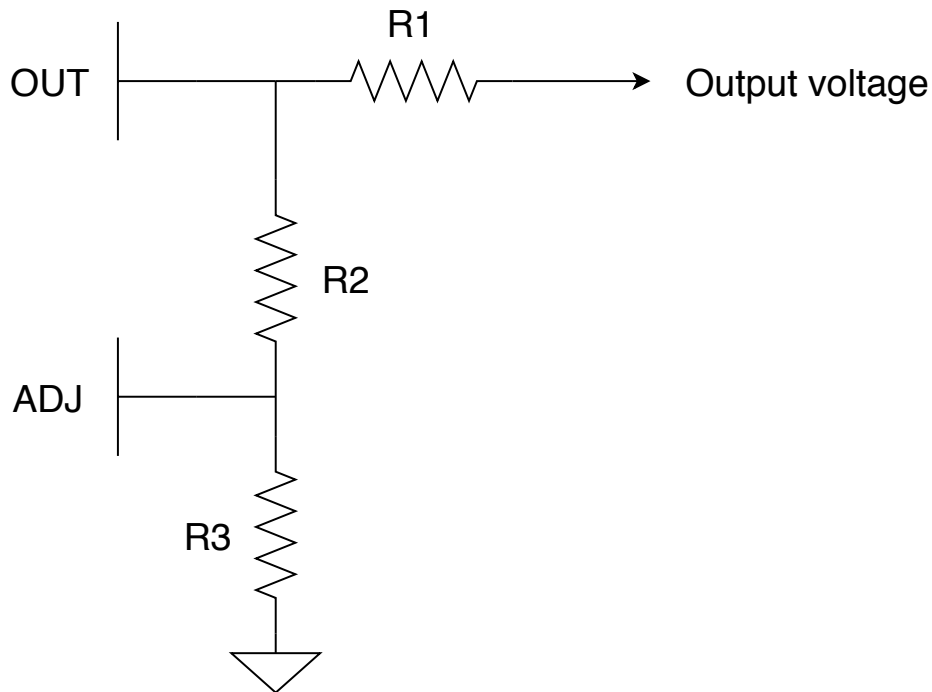


Figure A.11: Resistor network between the ADJ and VOUT pin

calculated as follow. Firstly, the upper and lower voltage levels can be expressed in equation A.8.

$$30 = 1.25 \left( 1 + \frac{R2 + R3}{R1} \right) \quad (A.8)$$

$$10 = 1.25 \left( 1 + \frac{R2}{R1} \right) \quad (A.9)$$

From this, the following expression can be deduced in equation A.10.

$$R1 = \frac{R3}{15} \quad (A.10)$$

$$R2 = 7R1 \quad (A.11)$$

With the minimum output current requirement in mind, the following resistor were calculated. Based on the availability of resistor values on the market, slightly different resistor values had to be implemented. These values are given in table A.1. The current going through the resistor at the minimum and maximum voltage level were calculated as

follow.

$$I_{adj}^{vout,max} = \frac{25}{750 + 62 + 432} \approx 20\text{mA} \quad (\text{A.12})$$

$$I_{adj}^{vout,min} = \frac{10}{62 + 432} \approx 20\text{mA} \quad (\text{A.13})$$

From this it can be deduced that the linear regulator can operate properly as the requirements were adhered to.

	Calculated	Chosen
R1	62.5 $\Omega$	62 $\Omega$
R2	437.5 $\Omega$	432 $\Omega$
R3	1000 $\Omega$	1000 $\Omega$

Table A.1: Table of the calculated and chosen value of the resistors

### A.14.3. Input and output capacitor

The input capacitor was recommended to be a 1  $\mu\text{F}$  capacitor and this recommendation was adhered to. However, the output capacitor is proportional to the output voltage as given in the datasheet of the regulator. From this, the optimal output capacitor value was chosen to be 2.5  $\mu\text{F}$ .

## A.15. PCB implementation of the deliverables

In this section, the design and implementation of the PCB's of the deliverables are discussed. Certain decisions that were made for the design of the PCB's are also explained. The area of the PCB's were strictly kept at a minimum as per requirement PER13-A

### A.15.1. PCB for the laser driver and bias voltage

Due to the bias voltage being a fixed voltage and for the sake of ease of implementation, it was decided to merge the laser driver PCB with the bias voltage PCB into one single PCB. Yet an option was implemented to separate the PCB into 2 separate PCB's, if either the bias voltage or the laser driver implementation malfunctions. From this, the total area of the PCB was 45 by 44 mm. Figure A.12 depicts the 3D model of the laser driver and bias voltage PCB

### A.15.2. PCB for the bus voltage

As already explained in section 4.5.1, the bus voltage is implemented using a linear regulator as the bus voltage is not fixed for a fixed frequency. With this in mind, it was decided to implement the bus voltage PCB as a single PCB and not to be merged with the bias voltage and laser driver PCB. The total area of the PCB was 50 by 30 mm and figure A.13 depicts the 3D model of the PCB.

### A.15.3. PCB for the APD bias

For the APD bias, the idea was to implement the PCB alongside the PCB with the transimpedance amplifier and the photodiode. Unfortunately due to time constraints and restriction of orthogonal testing, it was decided to implement the APD bias as a single PCB. The area of the PCB was 45 by 22 mm and figure A.14 depicts the 3D model of the APD bias PCB.

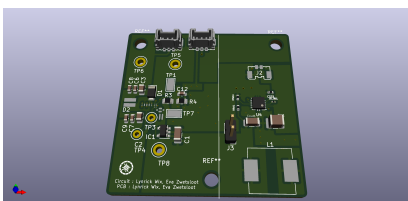


Figure A.12: 3D model of the laser driver and bias voltage PCB

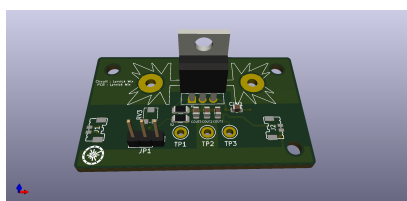


Figure A.13: 3D model of the bus voltage PCB

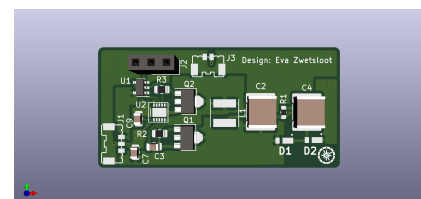


Figure A.14: 3D model of the APD bias PCB

## **A.16. Test plan for the altered laser driver**

A test plan was written in order to properly test the PCB's for the transmission stage. The test plan is further elaborated in the forthcoming sections.

### **A.16.1. Goal of the test**

The main goal of the test is to measure the inductance overshoot of the reference design of the laser driver from Texas Instrument and the altered version of the laser driver. Furthermore, the conditions for which a 1 ns pulse can be created will be set and documented for further validation of the altered laser driver. From each of these two goals, a conclusion will be drawn as which implementation is most suitable for operation within the LiDAR system.

### **A.16.2. List of essentials**

The following components and devices that are needed for this test are as follow :

1. Altered laser driver PCB
2. Bus voltage supply PCB
3. Power supply  
This will supply the 48 V to the system.
4. Function generator  
This will supply the necessary pulse signal for the pulse shortening buffer.
5. Oscilloscope  
This is to observe the pulse signal that is being created by the altered laser driver.
6. Necessary wires for connection between the PCB's, power supply, oscilloscope and the function generator.
7. Multimeter
8. Probe cable
9. Flat screwdriver  
This is needed to adjust the pulse width accordingly.
10. Masking tape
11. Canister tube  
This is to cover the setup from sunlight coming from outside, this is to better measure the optical output with the optical output meter.
12. Towel  
To cover the setup even more from the sunlight.

### **A.16.3. Testplan steps**

The following steps were taken to execute the test properly and with success

1. First connect all the necessary connection between the laser driver, bus voltage and oscilloscope
2. Use the multimeter to check the continuity of all the connections.
3. Check if the power supply for the bus voltage and the bias voltage is at the correct voltage level and safe for operation
4. Check if the voltage level, repetition rate and pulse width of the function generator is correct and safe for operation by using the oscilloscope
5. Connect the probe to the correct test point to depict the pulse width signal from the laser driver and on the oscilloscope
6. If all is well, turn the function generator on first and then the power supply
7. Observe the setup for 3 seconds to check whether or not an incorrect connection was made and if the PCB's can withstand the input signals.
8. After this step, observe the waveform from the probe on the oscilloscope

9. When the pulse width of the waveform is not 1 ns, adjust the pulse width using the onboard potentiometer of the laser driver.
10. Save the waveform onto a USB stick as a .CSV file if possible